UNCLASSIFIED

AD 402 079

Reproduced
by the

DEFENSE DOCUMENTATION CENTER

FOR

SCIENTIFIC AND TECHNICAL INFORMATION

CAMERON STATION, ALEXANDRIA, VIRGINIA

UNCLASSIFIED

APPROXIMATE SOLUTIONS OF THE LATERAL MOTION OF RE-ENTRY VEHICLES DURING CONSTANT ALTITUDE GLIDE

H. E. Wang

25 February 1963

Contract No. AF04(695)-169

ASTIA

APR 2 2 1963

AEROSPACE CORPORATION

APPROXIMATE SOLUTIONS OF THE LATERAL MOTION OF RE-ENTRY VEHICLES DURING CONSTANT ALTITUDE GLIDE

H. E. Wang

25 February 1963

Contract No. AF04(695)-169

AEROSPACE CORPORATION
2400 East El Segundo Boulevard
El Segundo, California

Prepared for

COMMANDER SPACE SYSTEMS DIVISION
UNITED STATES AIR FORCE
Inglewood, California

APPROXIMATE SOLUTIONS OF THE LATERAL MOTION OF
RE-ENTRY VEHICLES DURING CONSTANT ALTITUDE GLIDE

25 February 1963

Prepared by ⟨signature: Hung-En Wang⟩

H.E. Wang

Approved by ⟨signature⟩

S.T. Chu, Head
Re-entry Studies Section

⟨signature⟩

A. Mager
Acting Department Head,
Gas Dynamics
Director, Spacecraft Sciences

AEROSPACE CORPORATION
2400 East El Segundo Boulevard
El Segundo, California

ABSTRACT

Approximate analytic solutions have been obtained to the lateral motion of re-entry vehicles during constant altitude glide. The constant altitude glide is maintained by banking the vehicle about its velocity vector at a fixed angle of attack. Such a glide mode is often used in design studies to achieve lateral range but no simple analytic solutions have been available up to now. The approach taken here is to first treat the "flat earth" case and then include the spherical earth correction. Simple expressions have been obtained for the turn angle, lateral range angle and the down range angle. A comparison with exact numerical solutions shows that the approximate solutions are sufficiently accurate for preliminary design purposes.

The approximate solutions, although simple, contain all the characteristics of the glide mode in question. The results show that the lateral range, being a function of $W/(C_D A \rho)$, exhibits a maximum for a given L/D and initial velocity for the spherical earth case. In the flat earth case, the maximum exists for suborbital and orbital initial velocities and ceases to exist above a certain initial velocity depending on L/D. The down range also exhibits a maximum for a given L/D and initial velocity provided that the initial velocity is suborbital. The spherical earth correction on the lateral and down range has been shown to be small for low $W/(C_D A \rho)$, L/D and initial velocities and becomes significant when these parameters are high. All these findings agree with exact numerical solutions.

CONTENTS

ILLUSTRATIONS

I. INTRODUCTION

In many cases, a space vehicle entering the earth's atmosphere requires lateral range capability for landing at a specific site. To gain lateral range, the vehicle must be steered out of the original orbit plane and as a result one needs an understanding of the lateral motion of such a vehicle. Slye (Reference 1) has presented an analytical method for studying the lateral motion of re-entry vehicles flying equilibrium glide trajectories. While this class of trajectories is of great interest and importance in designing a re-entry flight path, its practical use is limited to re-entry from orbital speed. When the vehicle enters the atmosphere at superorbital speeds, a transition phase is required to bridge the gap between the superorbital initial phase and the suborbital equilibrium glide phase. One type of trajectory capable of carrying out this transition is the constant altitude glide. Constant altitude glide has drawn the attention of many designers; for example, Smith and Menard (Reference 2) used a constant altitude glide to maneuver for range near orbital speed. Ferri and Ting (Reference 3) also studied constant altitude glide to reduce the second peak deceleration and to control the vehicle from skipping. These authors, however, did not consider the advantage of obtaining lateral range by banking the vehicle while maintaining the constant altitude glide. Banking the vehicle not only produces lateral range but also ease the problem of designing a thermal protection system due to the fact that only one side of the vehicle is exposed to the free-stream. This subject has been discussed by Gervais, duPont and Lowe (Reference 3).

While the constant altitude glide is of great practical interest, it is not without problems to get a vehicle onto such a glide from the initial phase of the re-entry, especially when the speed is superorbital. It can be readily appreciated that lift modulation in the initial phase is required. Wang and Chu (Reference 4) have attempted to analytically solve the problem of re-entry trajectory with variable lift of a simple type. They have demonstrated that by varying the parameters in the lift program, one is indeed able to make a smooth transition from the initial plunge to a constant altitude glide. This can be done either by pitch control or by bank control. In the present paper, it will be assumed that the vehicle is already at the beginning of a constant altitude glide and the initial phase of the re-entry trajectory is beyond the scope of this analysis.

The particular maneuver to be dealt with here, namely, constant altitude glide by banking at a fixed angle of attack, has been studied by Skulsky (Reference 5). He presented exact numerical solutions to the equations of motion. Later, Wang and Skulsky (Reference 6) discussed the characteristics of the lateral range obtained during such a glide. Their discussion was based on the numerical solutions presented in Reference 5. The present paper presents, however, analytic solutions to the problem using a basic approximation. The approximation appears to be crude at first but the results turn out to be quite satisfactory. The "flat earth" solution will be given in the first part of the paper and in the second part the spherical earth case will be dealt with. A summary of the approximate solutions is given in Appendix A.

II. EQUATIONS OF MOTION

The three-dimensional equations of motion of a hypervelocity vehicle flying over a spherical earth have been derived by London (Reference 7), by Love and Neustadt (Reference 8), and by Wang (Reference 9). In Reference 9, the lateral centrifugal force term has been discussed extensively with regard to its origin and physical identity. It is not considered necessary to include the derivation of these equations in this paper. For constant altitude glide these equations reduce to

$$\left(\frac{2W}{C_D A \rho}\right) \frac{dV}{dt} = -gV^2 \tag{1}$$

$$V^2 \left(\frac{L}{D}\right) \cos \phi = \left(\frac{2W}{C_D A \rho}\right) \left[1 - \left(\frac{V}{V_s}\right)^2\right] \tag{2}$$

$$\frac{d\psi}{dt} = \left(\frac{L}{D}\right) \frac{Vg \sin \phi}{\left(\frac{2W}{C_D A \rho}\right)} - \frac{Vg \cos \psi \tan \lambda}{V_s^2} \tag{3}$$

Here ϕ is the bank angle measured from the vertical, ψ is the turn angle measured from the original heading and λ is the lateral range angle defined as the ratio of the lateral range to the radius of the earth (equal to 3440 nautical miles in the calculations shown later). These angles are shown in Figure 1. The other symbols have their usual meaning. Together with these three equations of motion, there are two kinematic equations:

$$\frac{d\lambda}{dt} = \frac{Vg \sin \psi}{V_s^2} \tag{4}$$

$$\frac{d\mu}{dt} = \frac{Vg \cos \psi}{V_s^2 \cos \lambda} \tag{5}$$

Here μ is the downrange angle as shown in Figure 1. It is to be noted that Equations (1), (2), and (3) are applicable for a point mass. A point mass vehicle is assumed in this analysis. The orbital speed V_s is assumed
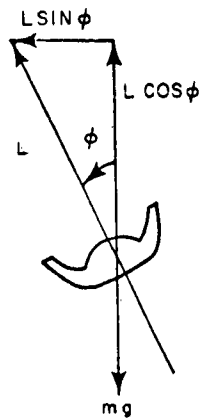
Figure 1a. Definition of Bank Angle ϕ.
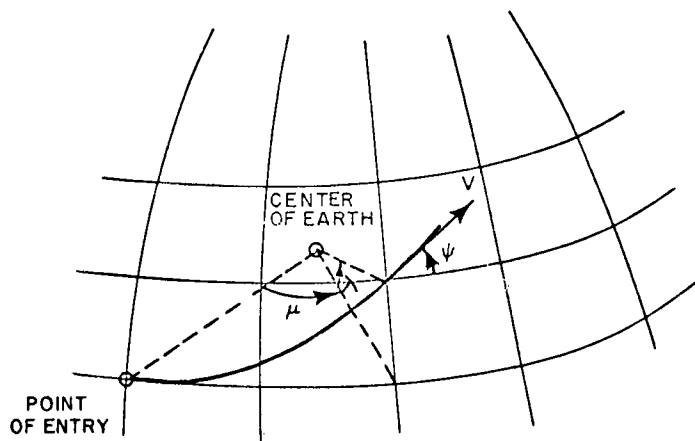(Velocity vector pointing into the paper)

Figure 1b. Definition of Turn Angle ψ, Lateral Range Angle λ, and Down Range Angle μ.

constant and equal to 26, 000 ft/sec in the numerical calculations given later in the paper.

If we write

$$B = \frac{W}{C_D A \rho} \tag{6}$$

and transform the independent variable from time t to velocity V through Equation (1), we obtain

$$- V \frac{d\psi}{dV} = \left(\frac{L}{D}\right) \sin \phi - \frac{2B}{V_s^2} \cos \psi \tan \lambda \tag{7}$$

$$- V \frac{d\lambda}{dV} = \frac{2B}{V_s^2} \sin \psi \tag{8}$$

$$- V \frac{d\mu}{dV} = \frac{2B}{V_s^2} \frac{\cos \psi}{\cos \lambda} \tag{9}$$

Denoting $\ln V = X$, these equations become

$$- \frac{d\psi}{dX} = \frac{L}{D} \sin \phi - \frac{2B}{V_s^2} \cos \psi \tan \lambda \tag{10}$$

$$- \frac{d\lambda}{dX} = \frac{2B}{V_s^2} \sin \psi \tag{11}$$

$$- \frac{d\mu}{dX} = \frac{2B}{V_s^2} \frac{\cos \psi}{\cos \lambda} \tag{12}$$

Equations (10), (11), and (12) determine the unknowns ψ, λ, and μ in terms of V. The bank angle ϕ can be readily written in terms of V by Equation (2) and the velocity V can be found as a function of t by integrating Equation (1). The main problem here is to solve the three nonlinear differential Equations

(10), (11), and (12). One can readily appreciate the difficulties associated with solving these equations analytically. The approach taken here is to treat the "flat earth" case first and then take up the spherical earth case. Flat earth means a condition when the second term on the right hand side of Equation (10) can be neglected. This term is proportional to the lateral centrifugal force. If the earth is truly flat, this term will of course drop out but so will the $(V/V_s)^2$ term in Equation (2). In the flat earth solution presented below, Equation (2) remains the way it is and only Equation (10) is simplified by neglecting the second term on the right hand side. By so doing, it does not result in a true flat earth as the name implies.

III. FLAT EARTH SOLUTION

For the flat earth case, although the equations to be solved are much simplified, they are still difficult to handle analytically because of the trigonometric functions involved. One certainly can eliminate $\sin \phi$ by Equation (2) and integrate Equation (10) and in principle it is integrable for the case of flat earth. But the resultant expression for ψ will be very complicated. In fact, this has been done by Skulsky (Reference 10), and one still has to use high speed computing machines to get a numerical value. As for λ and μ, numerical integration is unavoidable. What is done here is to further simplify Equation (10) by making the following approximation:

$$\sin \phi = 1 \tag{13}$$

Let us investigate this approximation. First, rewrite Equation (2) as follows:

$$\sin \phi = \sqrt{1 - C^2 \left[\left(\frac{V_s}{V} \right)^2 - 1 \right]^2} \tag{14}$$

where

$$C = \frac{2B}{\left(\frac{L}{D} \right) V_s^2} = 2W / (C_L A \rho V_s^2) \tag{15}$$

Equation (14) is plotted in Figure 2. It is seen in Figure 2 that for small values of C, $\sin \phi$ is practically equal to unity for a wide range of V/V_s. For example, when the initial velocity is $V_i/V_s = 1.2$ and $C = 0.1$, $\sin \phi$ is practically unity down to $V/V_s = 0.5$ and rapidly decreases to zero at $V_i/V_s = 0.3$. Integrating Equation (10) (when the second term on the right hand side is omitted for flat earth) is effectively to find the area under each $\sin \phi$ curve for various C. The approximation $\sin \phi = 1$ will give the area of the rectangle bounded by V_i/V_s and V_f/V_s where V_f is the final velocity that is at the end of the constant altitude glide where $\phi = 0$. This area will not be much larger than that under the actual $\sin \phi$ curve. For high C, the error should increase. For low initial velocities, the error should also increase. For example, when $V_i/V_s = 0.77$ and $C = 0.8$, there is no point where $\sin \phi$ is close to unity. Therefore,
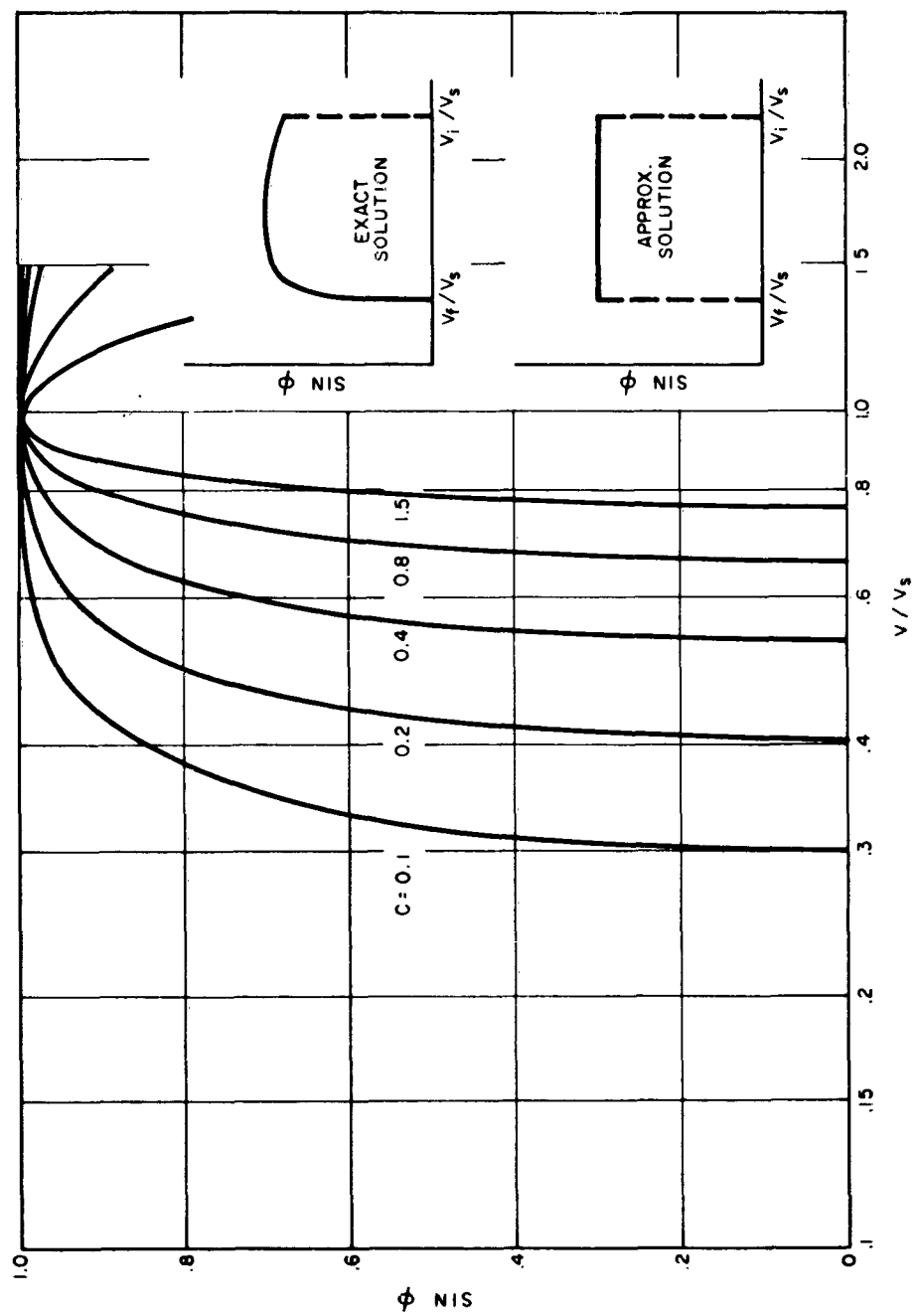
Figure 2. Variation of sin ϕ as a Function of V/V_s and C.

the approximation is the worst at high C and low initial velocities. The numerical examples given later in the paper bear this out but the inaccuracy in λ and μ is surprisingly low.

By this approximation $\sin \phi = 1$, Equation (10) for the flat earth case reduces to

$$-\frac{d\psi_0}{dX} = \frac{L}{D} \tag{16}$$

Here the subscript 0 denotes flat earth solution. The initial condition is $\psi_0 = 0$ at X_i. Integrating Equation (15) gives the following simple result.

$$\psi_0 = \frac{L}{D}(X_i - X) \tag{17}$$

or

$$\psi_0 = \frac{L}{D} \ln (V_i/V) \tag{18}$$

By Equation (17), Equation (11) can be integrated with the initial condition that $\lambda_0 = 0$ at X_i and the result is

$$\lambda_0 = C(1 - \cos \psi_0) \tag{19}$$

At the end of the constant altitude glide, the bank angle ϕ vanishes; that is to say, the vehicle has reached the saturation point and cannot maintain a constant altitude unless by changing the angle of attack. Since the flight mode considered here is constant altitude glide by banking at a fixed angle of attack, the final velocity must be determined by the condition $\phi = 0$. Therefore, by Equation (14), one has

$$V_f = \frac{V_s}{\sqrt{1 + \frac{1}{C}}} \tag{20}$$

The final turn angle and the final lateral range angle are respectively

$$\psi_{0f} = \frac{L}{D} \ln \frac{V_i}{V_s} \left[1 + \frac{1}{C} \right] \tag{21}$$

$$\lambda_{0f} = C (1 - \cos \psi_{0f}) \tag{22}$$

At this point, it is worthwhile to compare these simple solutions with exact numerical solutions. The exact numerical solutions are taken from References 5 and 10. Reference 10 gives the flat earth solutions and should serve as a check against the $\sin \phi = 1$ approximation. Reference 5 gives the spherical earth solution and should indicate the magnitude of the spherical earth effect.

Figure 3 is a plot of $\psi_{0f}/(L/D)$ as a function of $W/(C_L A \rho)$ for initial velocities 32,000, 26,000, and 20,000 ft/sec. Equation (21) predicts too high a turn angle as expected. The percentage error increases with increasing $W/(C_L A \rho)$ for a given initial velocity and decreases with increasing initial velocity for a given $W/(C_L A \rho)$. These are the expected nature of the approximation. The absolute magnitude of the error in the quantity $\psi_{0f}/(L/D)$ is of the order of 2 to about 6 degrees in the range compared. Generally speaking, the accuracy of the simple approximate solution is satisfactory; it correctly predicts the general trend and correctly establishes the functional dependence of ψ_{0f} upon B, L/D and V_i. Figures 4a, 4b and 4c show the same comparison plotted in a slightly different form. Included in these figures are the exact numerical solutions for spherical earth, which will be discussed later in Section IV.

A comparison of the lateral range is given in Figures 5a, 5b and 5c. For all three initial velocities, the approximate solution, Equation (22), agrees with the exact numerical solutions for flat earth well within 10 per cent. In some cases when the initial velocity is high, the present approximate solution is almost exact and so is it for low $W/(C_D A \rho)$. The general characteristics of the lateral range as a function of B, L/D and V_i including the peaks are
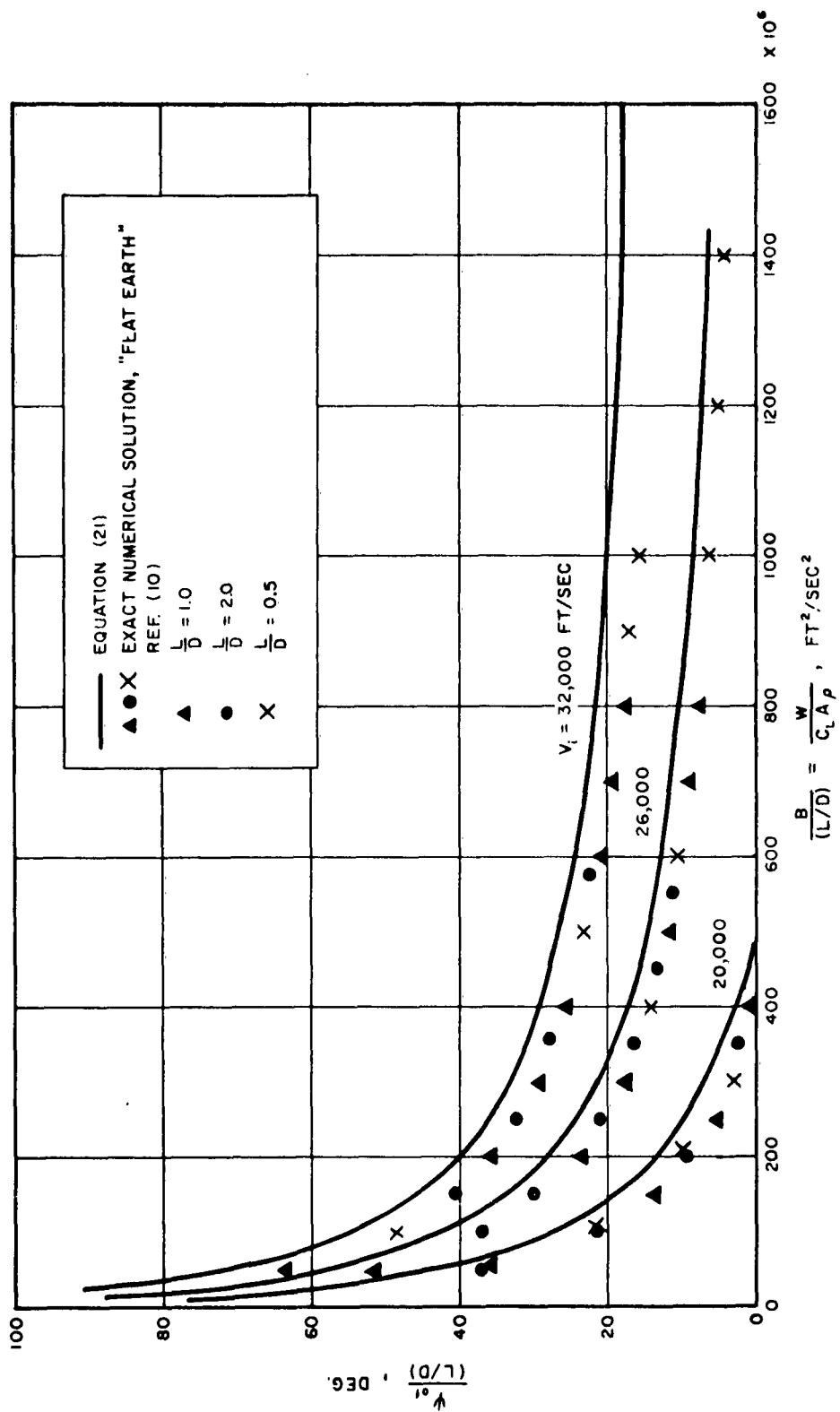
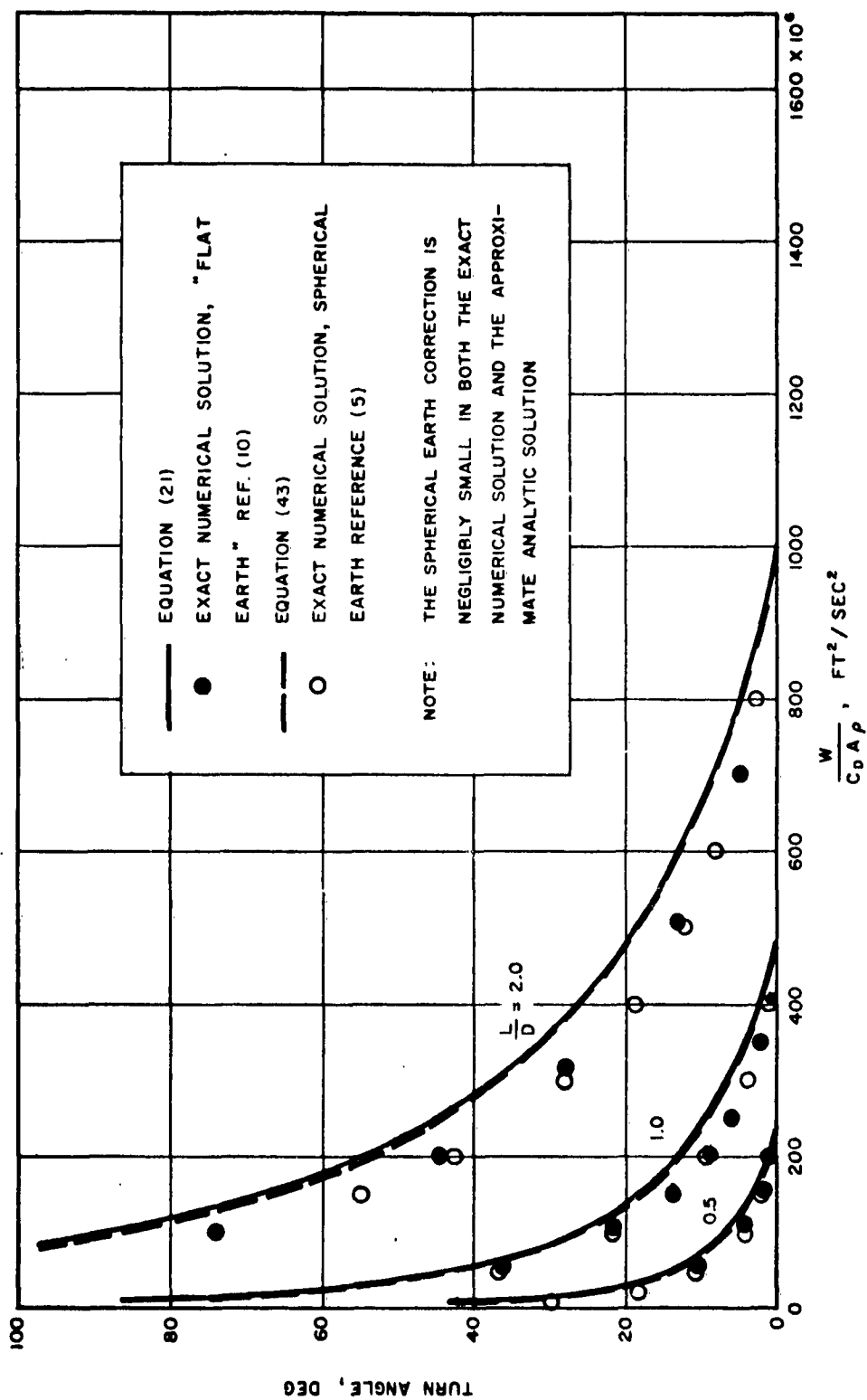Figure 3. Comparison of Final Turn Angle.

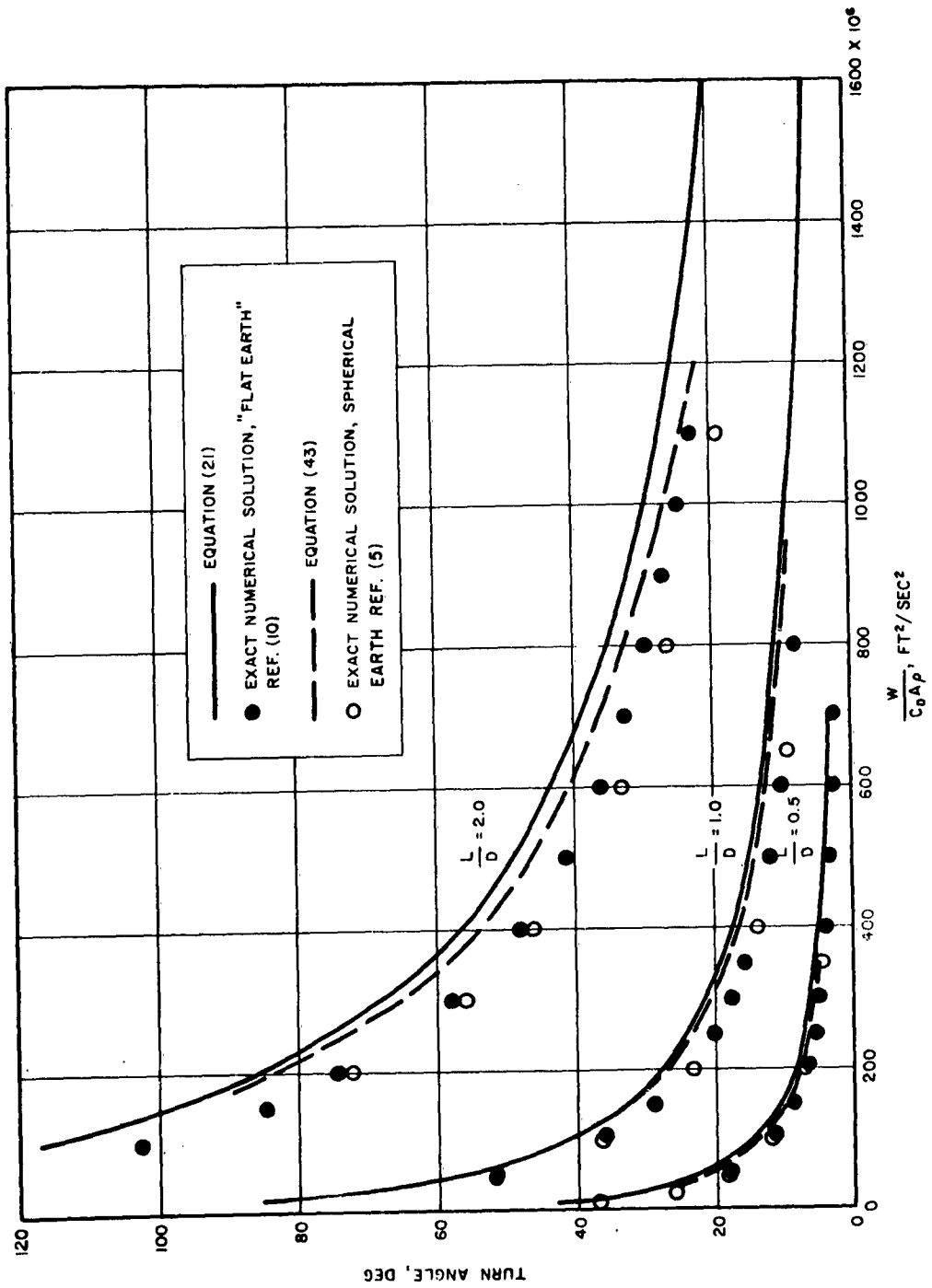Figure 4a. Comparison of Final Turn Angle ($V_i = 20,000$ ft/sec).

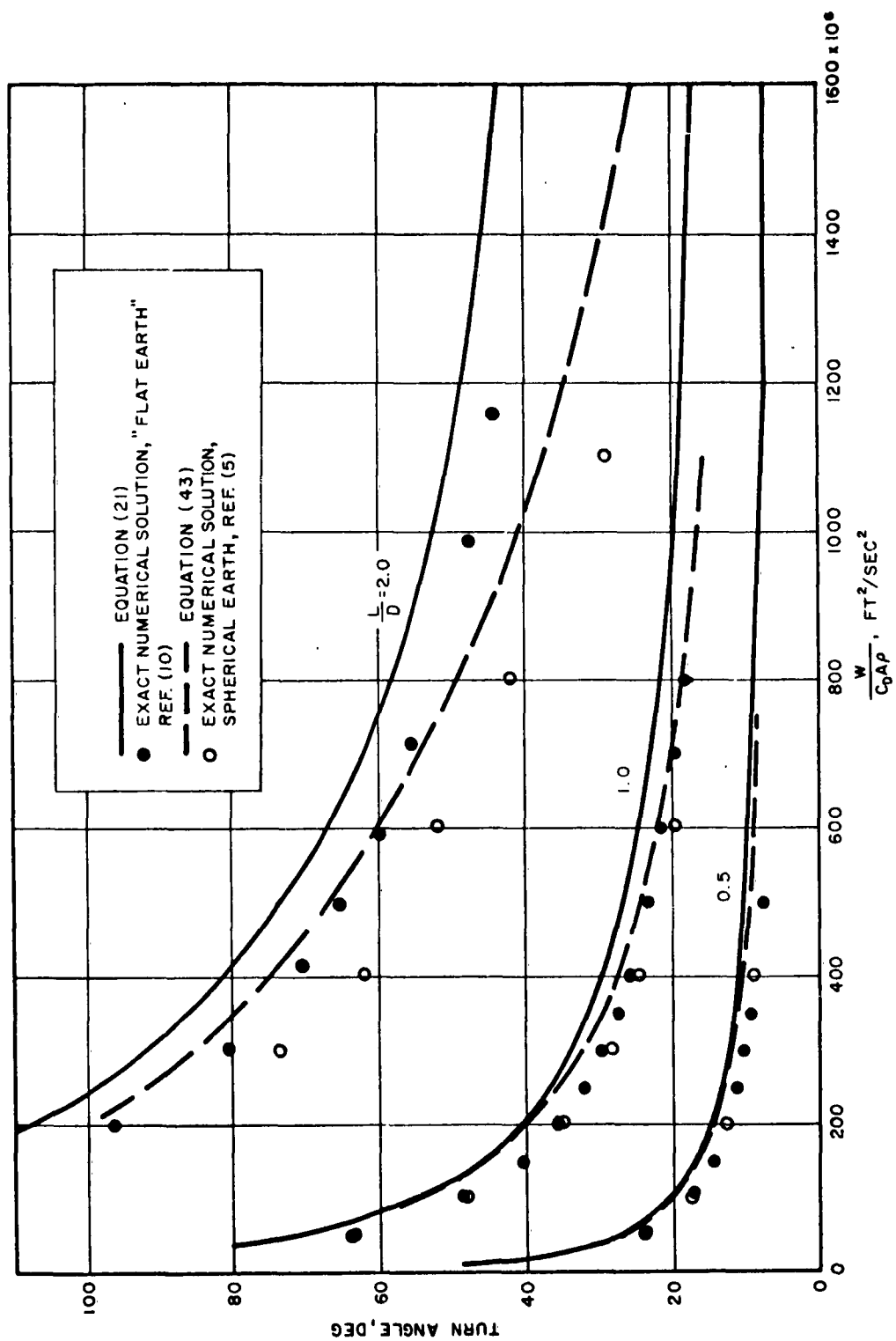Figure 4b. Comparison of Final Turn Angle (V_i = 26,000 ft/sec).

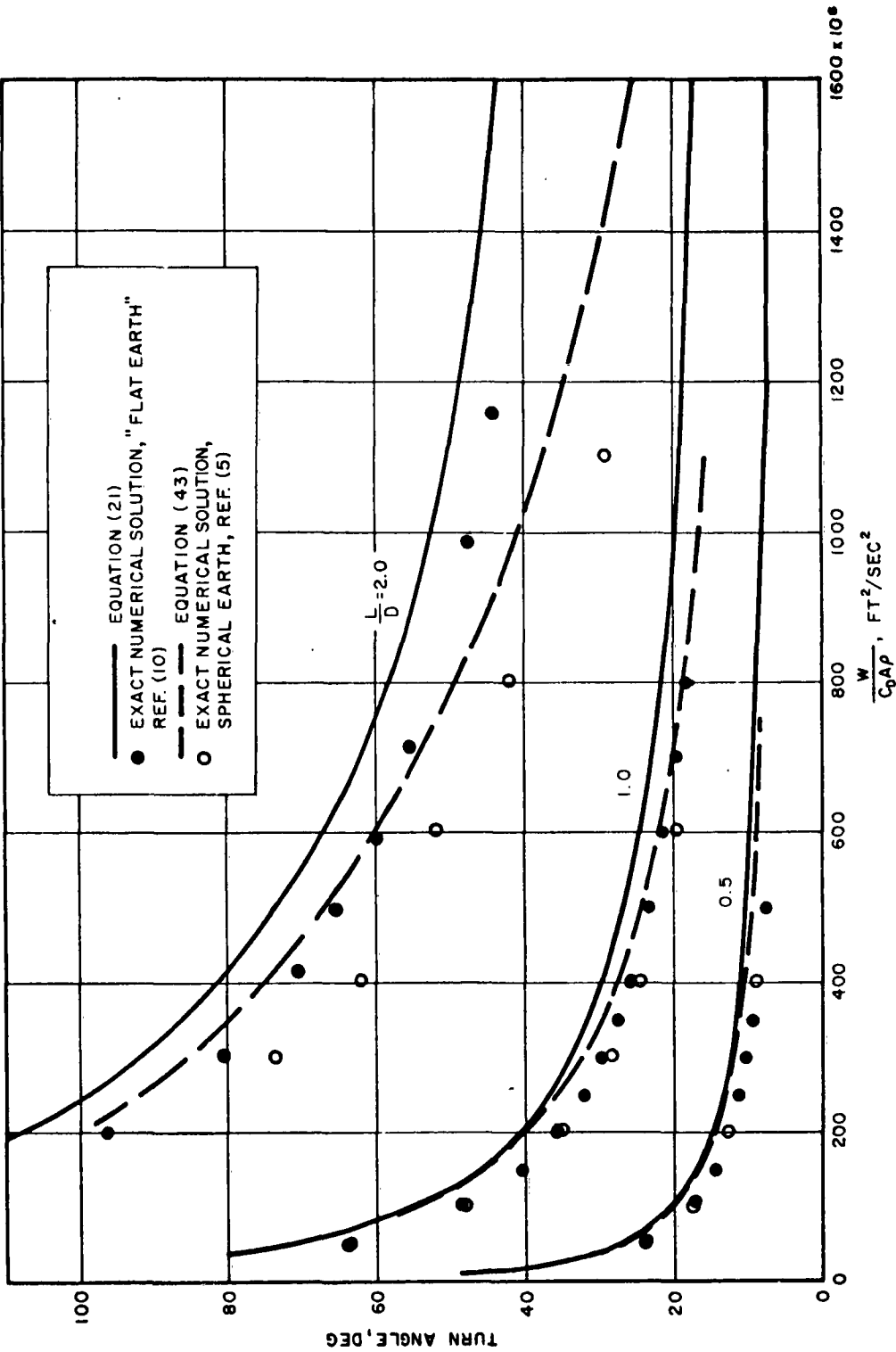Figure 4c. Comparison of Final Turn Angle (V_i = 32,000 ft/sec).

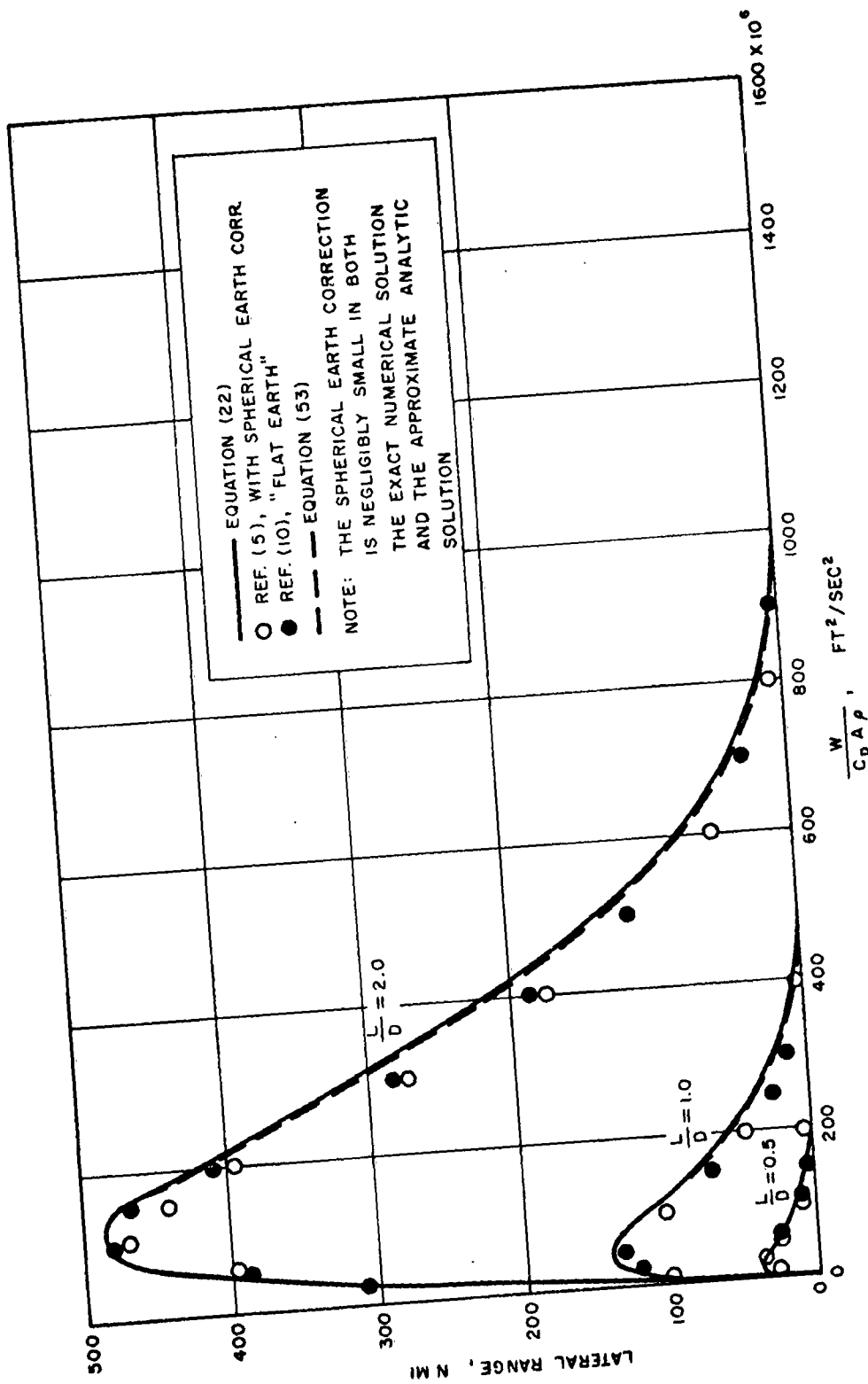Figure 4c. Comparison of Final Turn Angle (V_i = 32,000 ft/sec).

Figure 5a. Comparison of Lateral Range (V_i = 20,000 ft/sec).
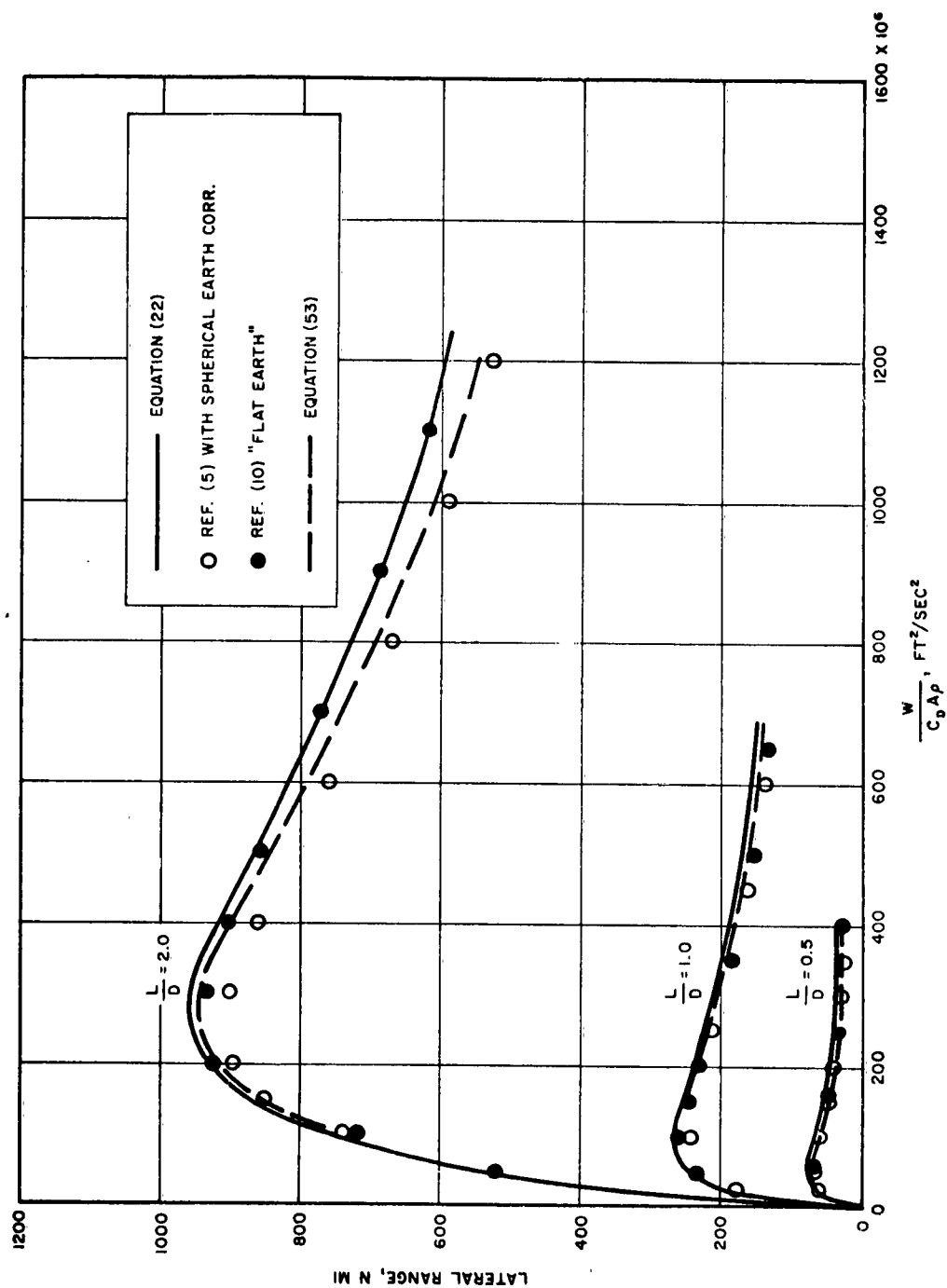
Figure 5b. Comparison of Lateral Range (V_i = 26,000 ft/sec).
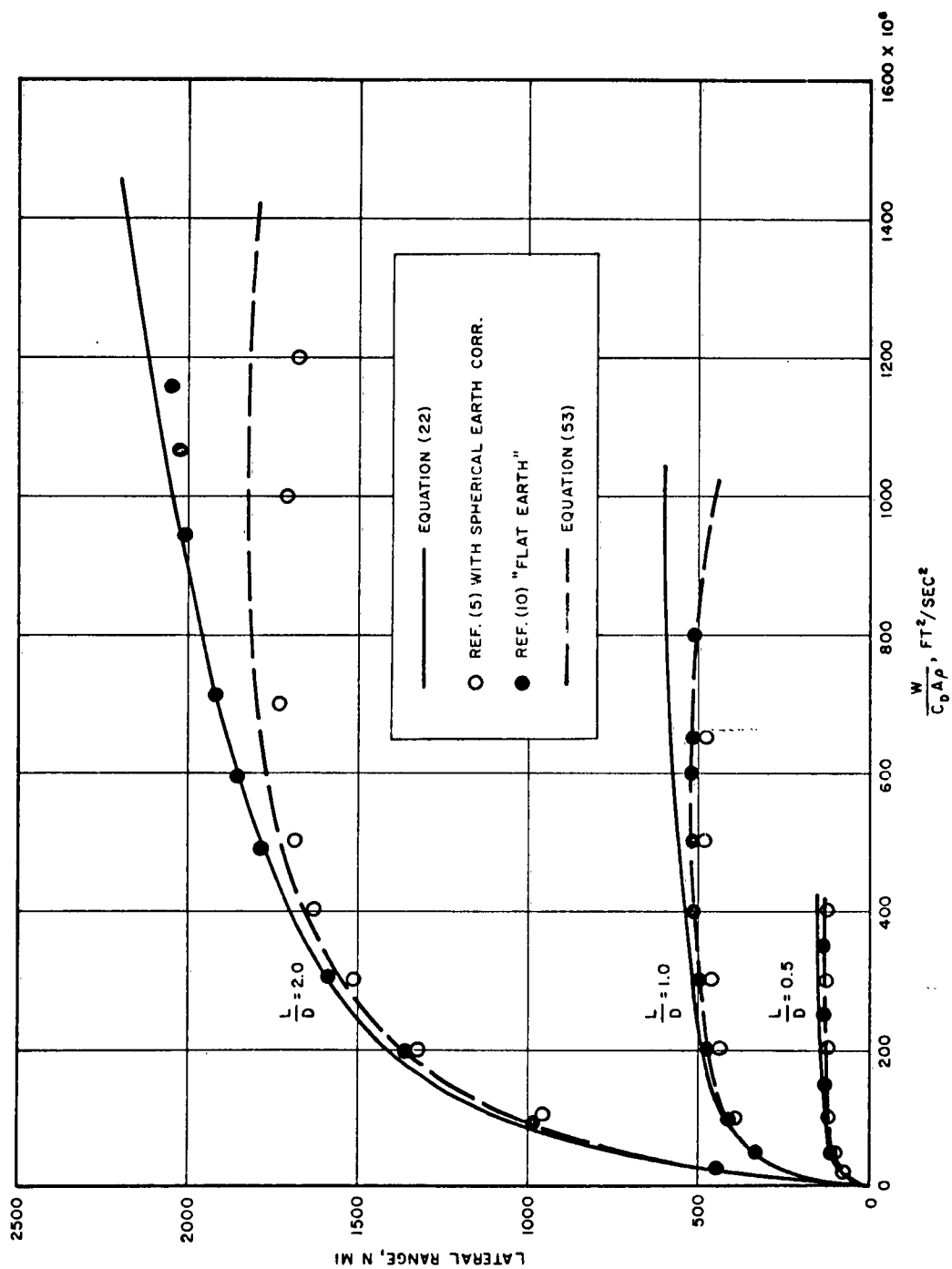
Figure 5c. Comparison of Lateral Range (V_i = 32,000 ft/sec).

well preserved in the approximate solution. The striking feature that one finds in these comparisons is that the accuracies of predicting ψ_{0f} and λ_{0f} are not at all the same. The approximate solution predicts the lateral range with a much higher accuracy than it does the turn angle. This can probably be explained in the following manner. For a given initial velocity and $W/(C_D A \rho)$, the exact flight path might be represented by the solid curve of Figure 6 while the approximate solution is indicated by the dashed line. Point A might represent the end of the turn. The lateral range in both computations might be very close to each other while the approximate solution predicts a much higher turn angle than the exact numerical solution.[+] This explanation is fully supported by the downrange prediction. The approximate solution always predicts a shorter downrange as will be seen later.

Let us now return to the development of the approximate solution. Equations (21) and (22) can be used to determine the maximum lateral range and the condition under which it occurs. Differentiating Equation (22) with respect to C and setting it equal to zero, one gets

$$\frac{d\lambda_{0f}}{dC} = (1 - \cos \psi_{0f}) + C \sin \psi_{0f} \frac{d\psi_{0f}}{dC} = 0 \tag{23}$$

where $d\psi_{0f}/dC$ can be found from Equation (21) as

$$\frac{d\psi_{0f}}{dC} = - \frac{1}{2} \frac{L}{D} \frac{1}{C(1 + C)} \tag{24}$$

Combining Equations (24) and (23), one gets

$$1 - \cos \psi_{0f}^* = \frac{1}{2} \frac{L}{D} \frac{\sin \psi_{0f}^*}{1 + C^*} \tag{25}$$

Here the * quantities denote the condition where the maximum lateral range occurs. Using the trigonometric relation of half angles and eliminating ψ_{0f}^* by Equation (21), Equation (25) finally reduces to

---

[+] Dr. Frank Billet analytically investigated the errors and showed similar results.
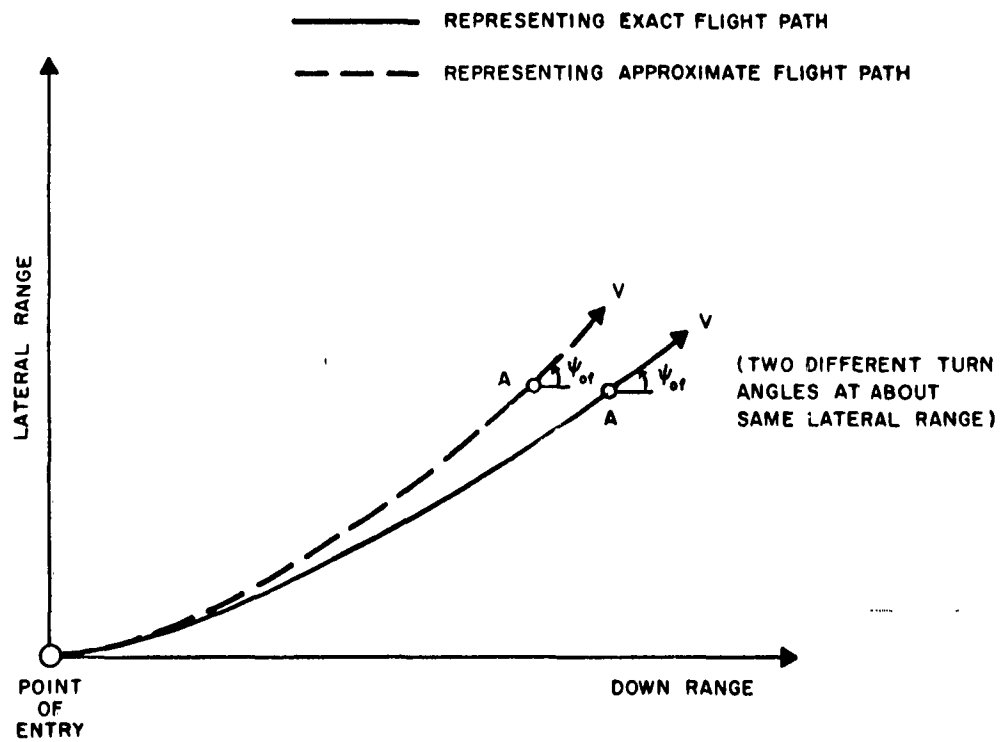
Figure 6. Schematic Diagram of the Exact and Approximate Flight Path.

$$\left(\frac{1}{2} \frac{L}{D}\right) \ln \frac{V_i}{V_s} \sqrt{1 + \frac{1}{C^*}} = \arctan \frac{\frac{1}{2} \frac{L}{D}}{1 + C^*} \qquad (26)$$

The maximum lateral range can be readily found to be

$$\lambda_{0f}^* = \left(\frac{1}{2} \frac{L}{D}\right) \frac{\sin \left\{ \frac{L}{D} \ln \left[\frac{V_i}{V_s} \right] \sqrt{1 + \frac{1}{C^*}} \right\}}{1 + \frac{1}{C^*}} \qquad (27)$$

These equations have been used to compute the maximum lateral range and where it occurs. The results are listed in Table 1. Included in Table 1 are also the exact numerical solutions. The comparison is extremely favorable. It is found that for a given L/D there exists an initial velocity beyond which there is no maximum for a flat earth. This is illustrated in Figure 7 in which Equation (26) is plotted.

The downrange angle can now be integrated. Dividing Equation (12) by Equation (11) one gets for flat earth,

$$\frac{d\mu_0}{d\lambda_0} = \frac{\cot \psi_0}{\cos \lambda_0} \qquad (28)$$

By Equation (19), one can write

$$\cot \psi_0 = \frac{C - \lambda_0}{\sqrt{C^2 - (C - \lambda_0)^2}} \qquad (29)$$

The $1/\cos \lambda_0$ term can be approximated by $1 + \frac{1}{2} \lambda_0^2$. This approximation is accurate within 5 per cent up to $\lambda_0 = 40$ degrees which means lateral range = 2400 nautical miles. In Figures 5a, 5b and 5c, the lateral range is smaller than 2400 nautical miles for all the conditions presented. If the lateral range

Table 1. Maximum Lateral Range and B* $(= \frac{1}{2} \frac{L}{D} V_s^2 C*)$.

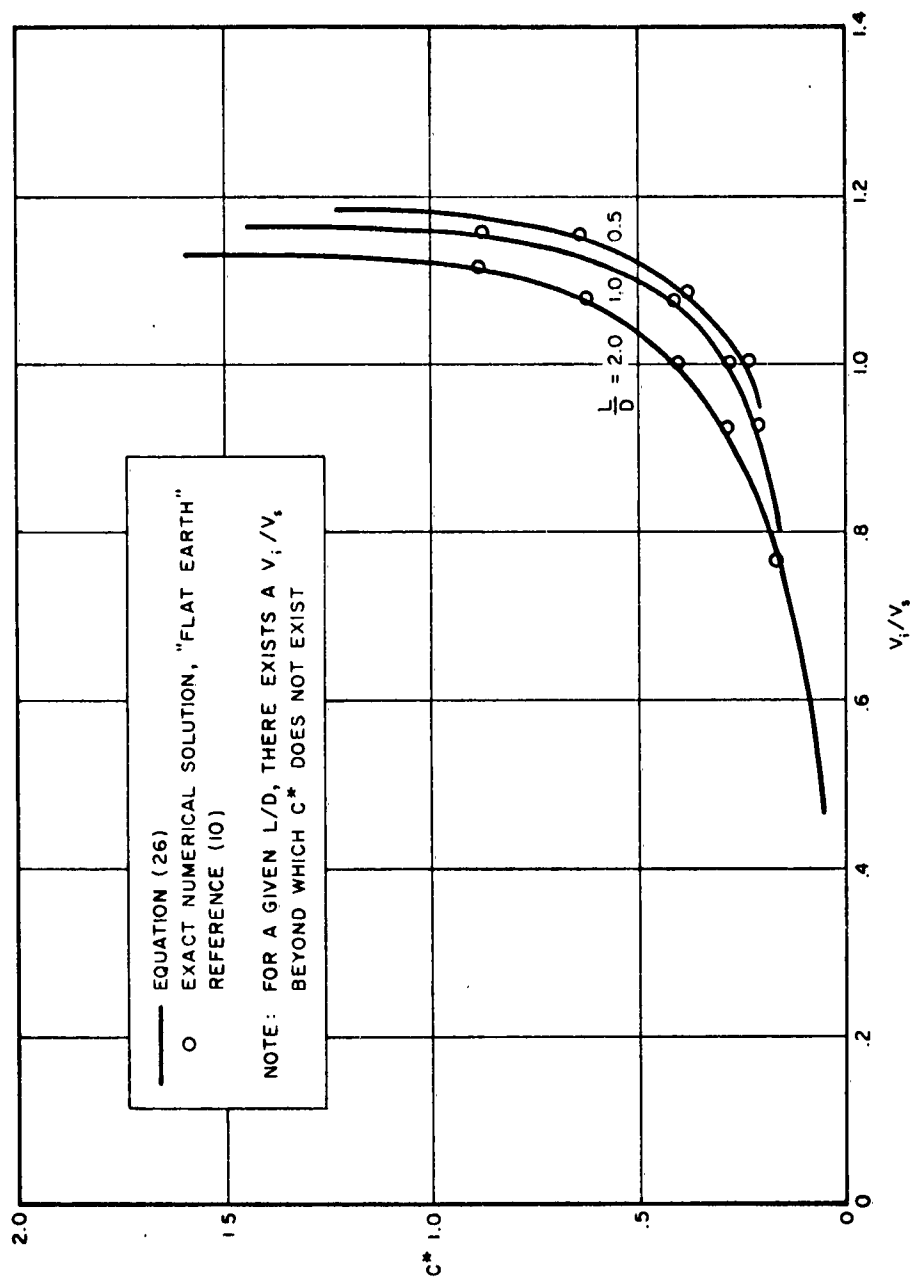| V_i ft/sec	L/D	"Flat Earth" Exact Numerical Solution		Approximate Solution	
		B* ft²/sec²	Maximum Lateral Range, naut mi	B* ft²/sec²	Maximum Lateral Range, naut mi
20,000	0.5	20 x 10⁶	35	20 x 10⁶	37
	1.0	50 x 10⁶	132	50 x 10⁶	140
	2.0	115 x 10⁶	485	115 x 10⁶	490
26,000	0.5	50 x 10⁶	65.5	50 x 10⁶	72
	1.0	95 x 10⁶	225	98 x 10⁶	265
	2.0	265 x 10⁶	937	275 x 10⁶	956
32,000	0.5	-	-	-	-
	1.0	-	-	-	-
	2.0	-	-	-	-

Figure 7. Comparison of C*, "Flat Earth".

is of the order of 1000 nautical miles, the approximation has an inaccuracy of about 1 per cent. Together with this approximation, Equations (28) and (29) combine to yield

$$\frac{d\mu_0}{d\lambda_0} = \frac{(C - \lambda_0)(1 + \frac{1}{2}\lambda_0^2)}{\sqrt{C^2 - (C - \lambda_0)^2}} \tag{30}$$

The initial condition is $\mu_0 = 0$ at $\lambda_0 = 0$. One finally gets by integrating Equation (30)

$$\mu_{0f} = \left(1 + \frac{C^2}{2} + \frac{C\lambda_{0f}}{2}\right) G - \frac{G^3}{6} + \frac{C^3}{2}\left\{arc\ sin\left(1 - \frac{\lambda_{0f}}{C}\right) - \frac{\pi}{2}\right\} \tag{31}$$

where

$$G = \sqrt{C^2 - (C - \lambda_{0f})^2} \tag{32}$$

In terms of ψ_{0f}, Equation (31) becomes

$$\mu_{0f} = C \sin \psi_{0f} + C^3\left(\sin \psi_{0f} - \frac{1}{2}\psi_{0f} - \frac{1}{4}\sin 2\psi_{0f} - \frac{\sin^3 \psi_{0f}}{6}\right) \tag{33}$$

For practical purposes, Equation (33) can be approximated by

$$\mu_{0f} = C \sin \psi_{0f} \tag{34}$$

Equation (34) agrees with Equation (33) within 1 per cent for lateral range up to 1000 nautical miles and within 3.5 per cent up to 2000 nautical miles. Note that Equation (34) would be the result of the integration if $\cos \lambda_0 = 1$ were assumed. The downrange is plotted in Figures 8a, 8b and 8c. Comparison with the exact numerical solutions show that the approximate solution predicts shorter downrange as depicted by the schematics of Figure 6, but the accuracy is very high. In these plots, Equation (34) is used except for a few points where
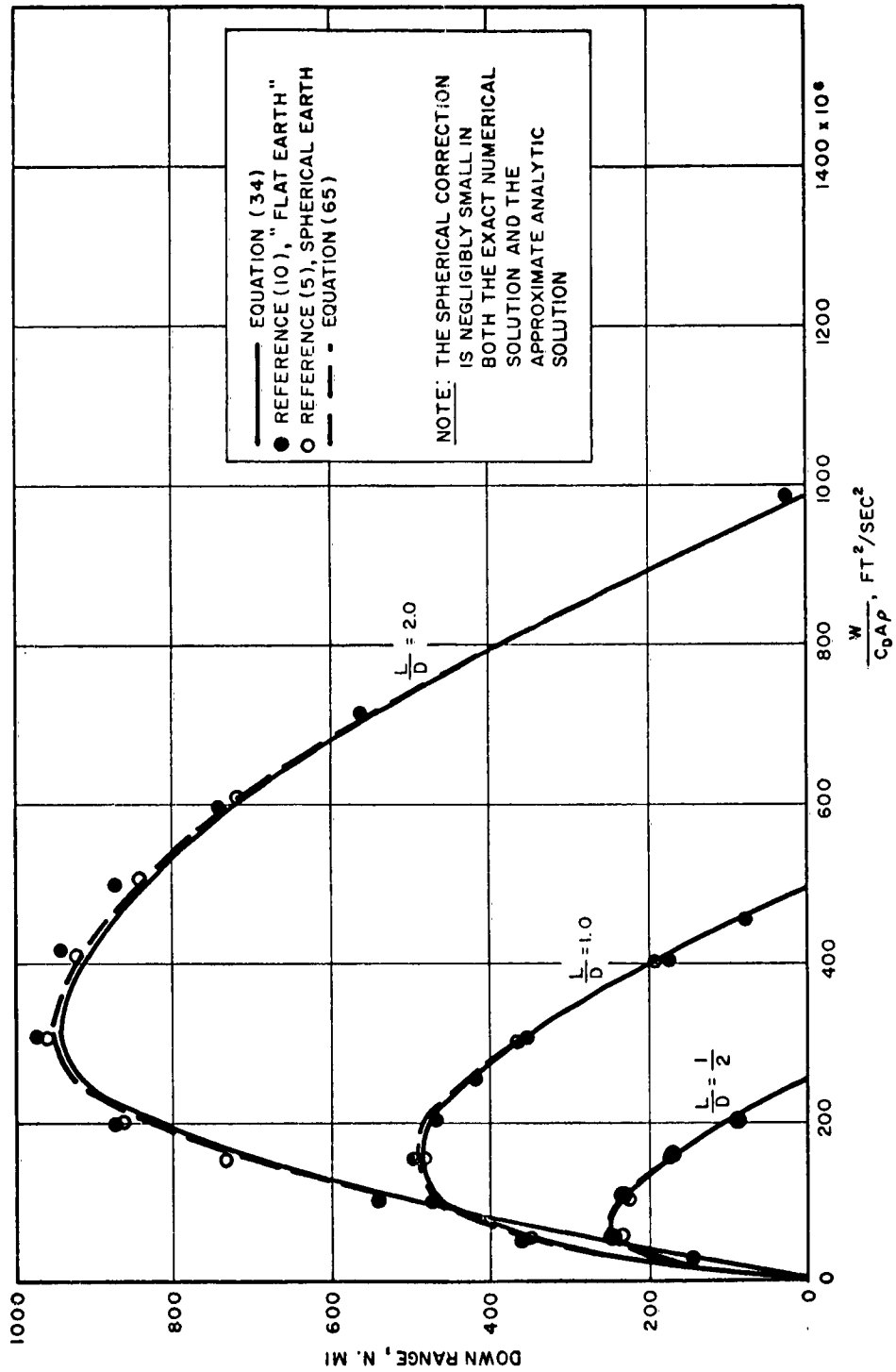
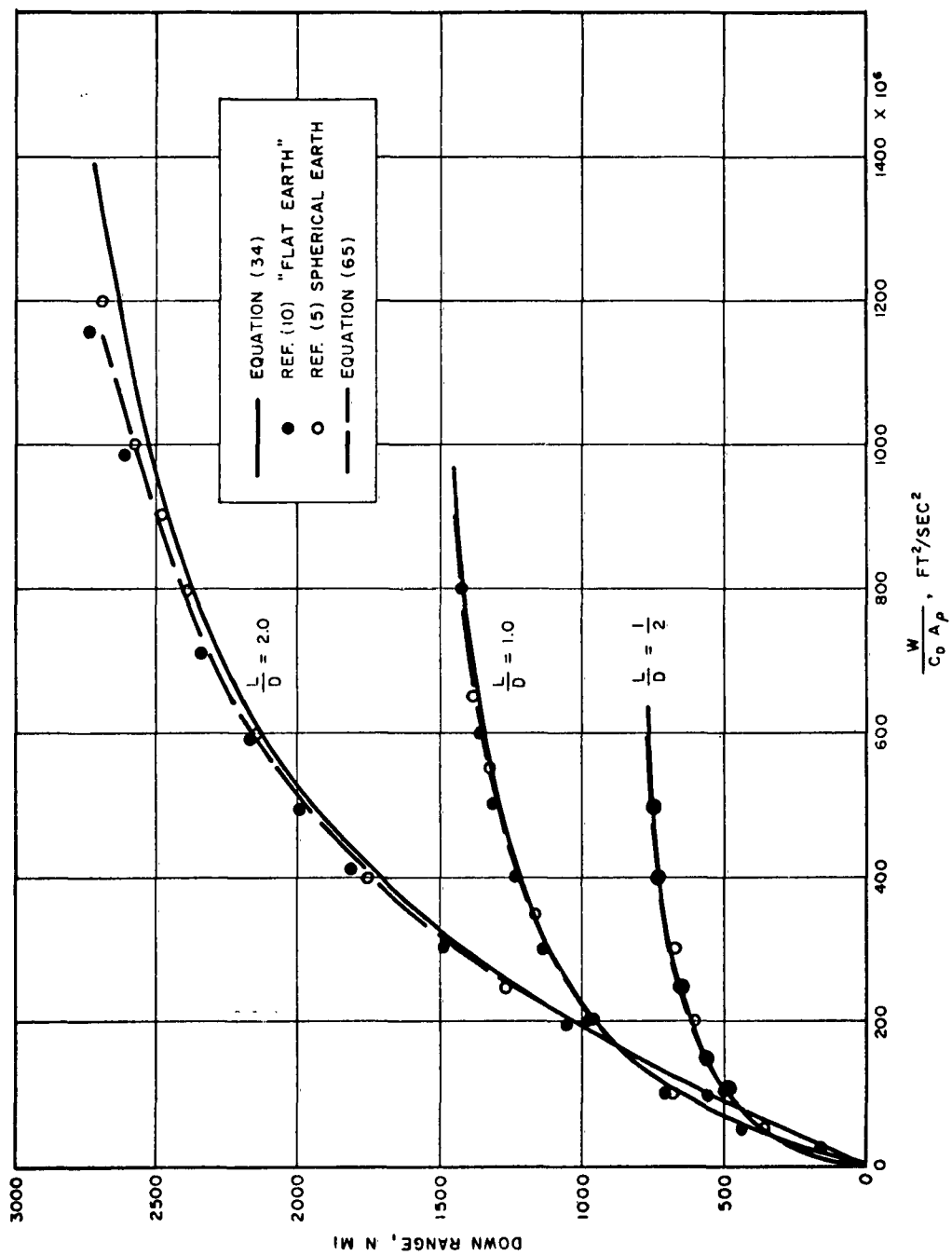Figure 8a. Comparison of Down Range ($V_i = 20,000$ ft/sec).
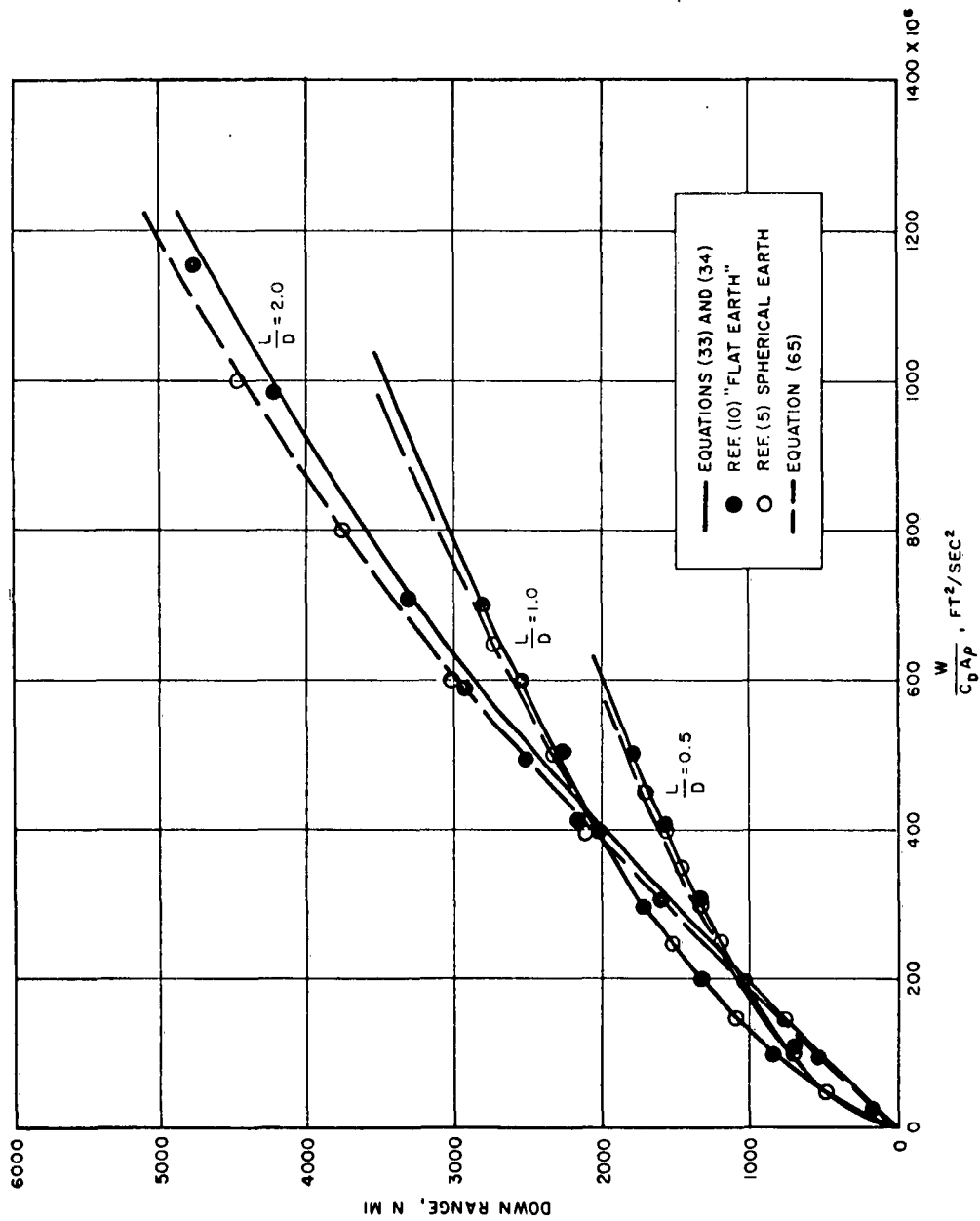
Figure 8b. Comparison of Down Range (V_i = 26,000 ft/sec).

Figure 8c. Comparison of Down Range ($V_i = 32,000$ ft/sec).

the lateral range is above 1500 nautical miles. It is observed that for a sub-orbital initial velocity, there exists a maximum down range. No maximum exists for orbital or superorbital initial velocities because the vehicle, at these speeds, can always fly at a sufficiently high altitude and go around the earth as many times as desired. This would produce no maximum on down-range. It is also noted that the maximum down range and maximum lateral range do not occur at the same altitude for a given vehicle. The maximum down range occurs at a higher altitude. One can readily find the maximum down range at suborbital initial velocities by differentiating Equation (34) and following the usual procedures. The result is given in Appendix A.

For completeness, the total flight time is given below. This is obtained by integrating Equation (1) with the initial condition $t = 0$ at V_i and the final condition $t = t_f$ at V_f.

$$t_f = \frac{L}{D} \frac{C}{g} V_s \left(\sqrt{1 + \frac{1}{C}} - \frac{V_s}{V_i} \right) \tag{35}$$

This essentially completes the development of the flat earth solution. It must be pointed out, however, that the solutions presented above must be used with caution when $W/(C_D A \rho)$ becomes very small. In the previous figures, the lateral and down range have been extended to zero at $W/(C_D A \rho) = 0$ by smooth curves. This was done as a matter of convenience. Strictly speaking, this is incorrect. As one can readily see that for a given L/D and initial velocity, the down range and lateral range expressions Equations (22) and (34) can be combined to yield an equation of a circle with its center at $\lambda = C$ and radius equal to C. When C is extremely small, although this may never become the case in practice, the vehicle can circle around the $\lambda = C$ location without gaining much lateral range and down range. The lateral range and down range curves must have an oscillatory nature at very small $W/(C_D A \rho)$. A more detailed discussion is given in Appendix B.

IV. SPHERICAL EARTH SOLUTION -
SPHERICAL EARTH CORRECTION

As can be seen from Figures 4, 5 and 8, the exact numerical solutions for spherical earth deviate only slightly from those for flat earth when the initial velocity is low. For example, when V_i = 20,000 ft/sec, one can hardly see any difference. This is true for the turn angle, the lateral range as well as the down range. When V_i = 26,000 ft/sec, the spherical earth solution begins to show some difference. The difference on lateral range is about 10 per cent at $W/(C_D A \rho)$ = 1000 x 10^6 ft^2/sec^2 and L/D = 2. The spherical earth solution shows higher difference at higher initial velocities. For example, when V_i = 32,000 ft/sec, the spherical earth solutions deviate from the flat earth solutions on lateral range by about 20 per cent at $W/(C_D A \rho)$ = 1000 x 10^6 ft^2/sec^2 and L/D = 2. This order of magnitude of the error produced by the flat earth solution is too high to be ignored and must be taken into consideration. On the other hand, an error of 20 per cent or so can still be treated mathematically as a second order. Thus, the second term on the right hand side of Equation (10) can be treated as a small perturbation on the first term. Accepting this idea, one is justified to speak of a spherical earth correction and treat it accordingly.

In the case of an equilibrium glide trajectory, Slye's solutions (Reference 1) are for flat earth. The spherical earth correction in that case has been discussed by Jackson (Reference 11) and by London (Reference 12). London advanced an argument that the proper criterion for determining the validity of the flat earth solution is the relative magnitude of the integrated lateral centrifugal force to the integrated lateral aerodynamic force, while the magnitude of the lateral range is not in itself a sufficient criterion. In the present case, we also observe that it is not sufficient to say when λ is small, the lateral centrifugal force term can be dropped from Equation (10). If one tries to do this, he will run into difficulties, because the first term (L/D) sin ϕ tends to zero toward the end of the glide while the second term $(2B \cos \psi \tan \lambda)/V_s^2$ can be very large. However, if one compares the integrated values of the term (L/D) sin ϕ and the term $(2B \cos \psi \tan \lambda)/V_s^2$, he will find that for most cases the latter will be smaller than the former. If the latter is so small that one can neglect it, the flat earth solution becomes valid.

The spherical earth correction for constant altitude glide has been discussed in Reference 6 where an empirical correlation was given for $L/D = 2$. What will be done here is to find an analytic expression for this correction within the present framework of approximation. Let us write

$$\psi = \psi_0 + \psi_1 \tag{36}$$

thus

$$\frac{d\psi}{dX} = \frac{d\psi_0}{dX} + \frac{d\psi_1}{dX} \tag{37}$$

Combining Equations (10) and (37), one has

$$-\frac{d\psi_0}{dX} - \frac{d\psi_1}{dX} = \frac{L}{D} \sin \phi - \frac{2B}{V_s^2} \cos \psi \tan \lambda \tag{38}$$

By the $\sin \phi = 1$ approximation, the first term on both sides of the equation cancels each other and one gets

$$\frac{d\psi_1}{dX} = \frac{2B}{V_s^2} \cos \psi \tan \lambda \tag{39}$$

With fairly good accuracy, one can replace $\cos \psi$ and $\tan \lambda$ by $\cos \psi_0$ and λ_0, respectively, and get

$$\frac{d\psi_1}{dX} = \frac{2B \lambda_0}{V_s^2} \cos \psi_0 \tag{40}$$

or

$$d\psi_1 = -C^2 (1 - \cos \psi_0) \cos \psi_0 \, d\psi_0 \tag{41}$$

The initial condition is $\psi_1 = 0$ and $\psi_0 = 0$. Integrating Equation (41) yields

$$\psi_{1f} = -C^2 \left(\sin \psi_{0f} - \frac{1}{2} \psi_{0f} - \frac{1}{4} \sin 2 \psi_{0f} \right) \tag{42}$$

Equation (42) relates the spherical earth correction and the flat earth solution. It is noted that ψ_{1f} is proportional to C^2 and it is always negative. Equation (42) is plotted in Figure 9 and also tabulated in Table 2. Applying this correction, the approximate spherical earth solution becomes

$$\psi_f = \psi_{0f} - C^2 \left(\sin \psi_{0f} - \frac{1}{2} \psi_{0f} - \frac{1}{4} \sin 2 \psi_{0f} \right) \tag{43}$$

where ψ_{0f} has been given by Equation (21). For comparison, Equation (43) is plotted in Figures 4a, 4b and 4c as the dashed lines. The comparison is quite favorable.

The spherical earth correction on lateral range is found as follows. With Equation (36) one can write Equation (11) as

$$-\frac{d\lambda}{dX} = \frac{2B}{V_s^2} \sin (\psi_0 + \psi_1) \tag{44}$$

$$-\frac{d\lambda}{dX} = \frac{2B}{V_s^2} (\sin \psi_0 \cos \psi_1 + \cos \psi_0 \sin \psi_1) \tag{44}$$

Since ψ_1 is small, one is justified to assume

$$\cos \psi_1 = 1 \text{ and } \sin \psi_1 = \psi_1 \tag{45}$$

Thus,

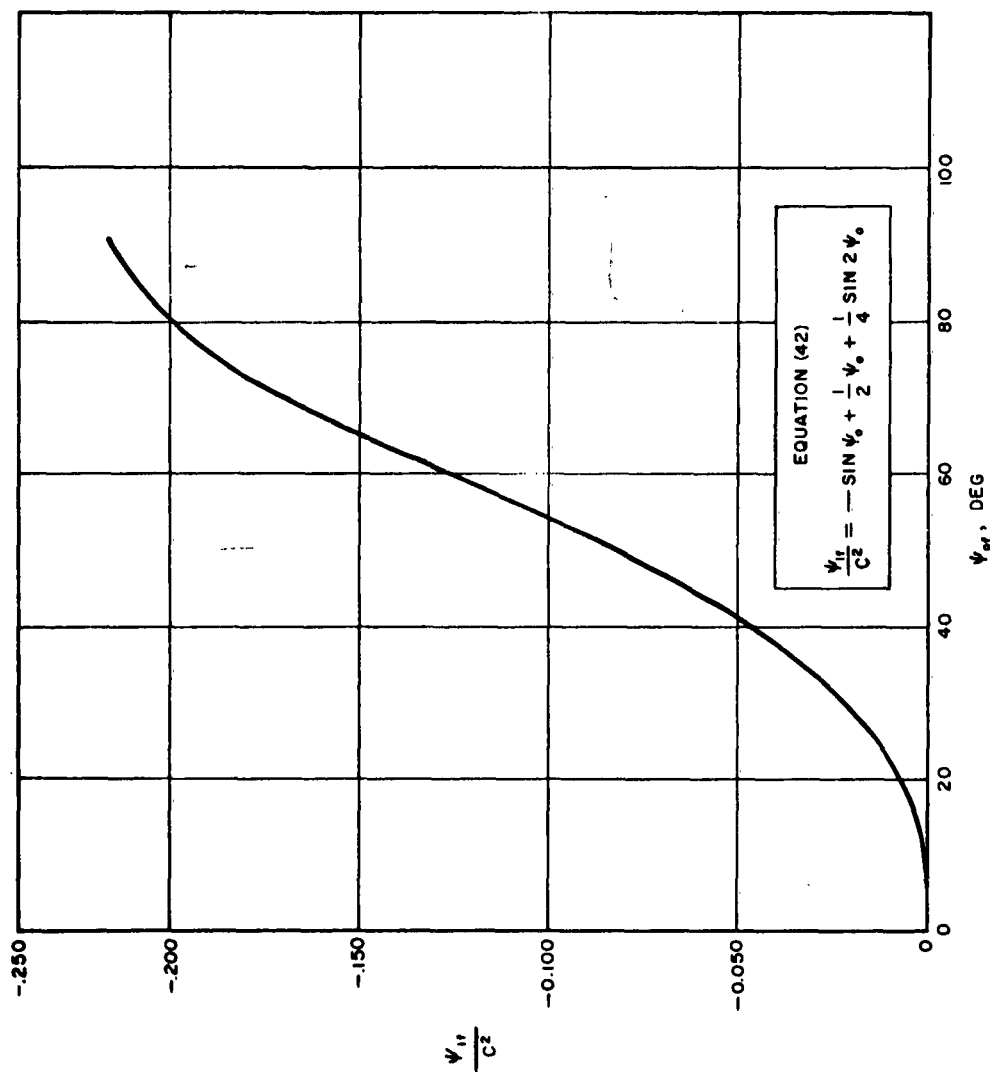$$-\frac{d\lambda}{dX} = \frac{2B}{V_s^2} \sin \psi_0 + \frac{2B}{V_s^2} \psi_1 \cos \psi_0 \tag{46}$$

$$\frac{\psi_{1r}}{C^2} = -\sin \psi_o + \frac{1}{2} \psi_o + \frac{1}{4} \sin 2 \psi_o$$

EQUATION (42)

Figure 9. Spherical Earth Correction on Turn Angle.

Table 2. Spherical Earth Correction on Turn Angle.

ψ_{0f} (deg)	ψ_{0f}/C^2 (deg)
0	0
10	- 0.063
20	- 0.384
30	- 1.245
40	- 2.728
50	- 4.710
60	- 7.175
70	- 9.65
80	- 11.48
90	- 12.33

Table 2. Spherical Earth Correction on Turn Angle.

ψ_{0f} (deg)	ψ_{0f}/C^2 (deg)
0	0
10	- 0.063
20	- 0.384
30	- 1.245
40	- 2.728
50	- 4.710
60	- 7.175
70	- 9.65
80	- 11.48
90	- 12.33

Following Equation (36), one can write

$$\lambda = \lambda_0 + \lambda_1 \tag{47}$$

and Equation (46) is reduced to

$$-\frac{d\lambda_0}{dX} - \frac{d\lambda_1}{dX} = \frac{2B}{V_s^2} \sin \psi_0 + \frac{2B}{V_s^2} \psi_1 \cos \psi_0 \tag{48}$$

Cancelling the flat earth terms, i. e.,

$$-\frac{d\lambda_0}{dX} = \frac{2B}{V_s^2} \sin \psi_0 \tag{49}$$

one gets for the spherical earth correction

$$\frac{d\lambda_1}{dX} = -\frac{2B}{V_s^2} \psi_1 \cos \psi_0 \tag{50}$$

or

$$d\lambda_1 = C^3 \cos \psi_0 \left(-\sin \psi_0 + \frac{\psi_0}{2} + \frac{\sin 2\psi_0}{4} \right) d\psi_0 \tag{51}$$

The initial condition is $\lambda_1 = 0$ at $\psi_0 = 0$. One finally gets by integrating Equation (51)

$$\lambda_{1f} = -C^3 \left(\frac{5}{6} + \frac{1}{6} \cos^3 \psi_{0f} - \frac{1}{2} \cos^2 \psi_{0f} - \frac{1}{2} \cos \psi_{0f} - \frac{1}{2} \psi_{0f} \sin \psi_{0f} \right) \tag{52}$$

Equation (52) is plotted in Figure 10 and also tabulated in Table 3. Note that λ_{1f}, being negative, is proportional to C^3. Applying this correction, the approximate spherical earth solution becomes
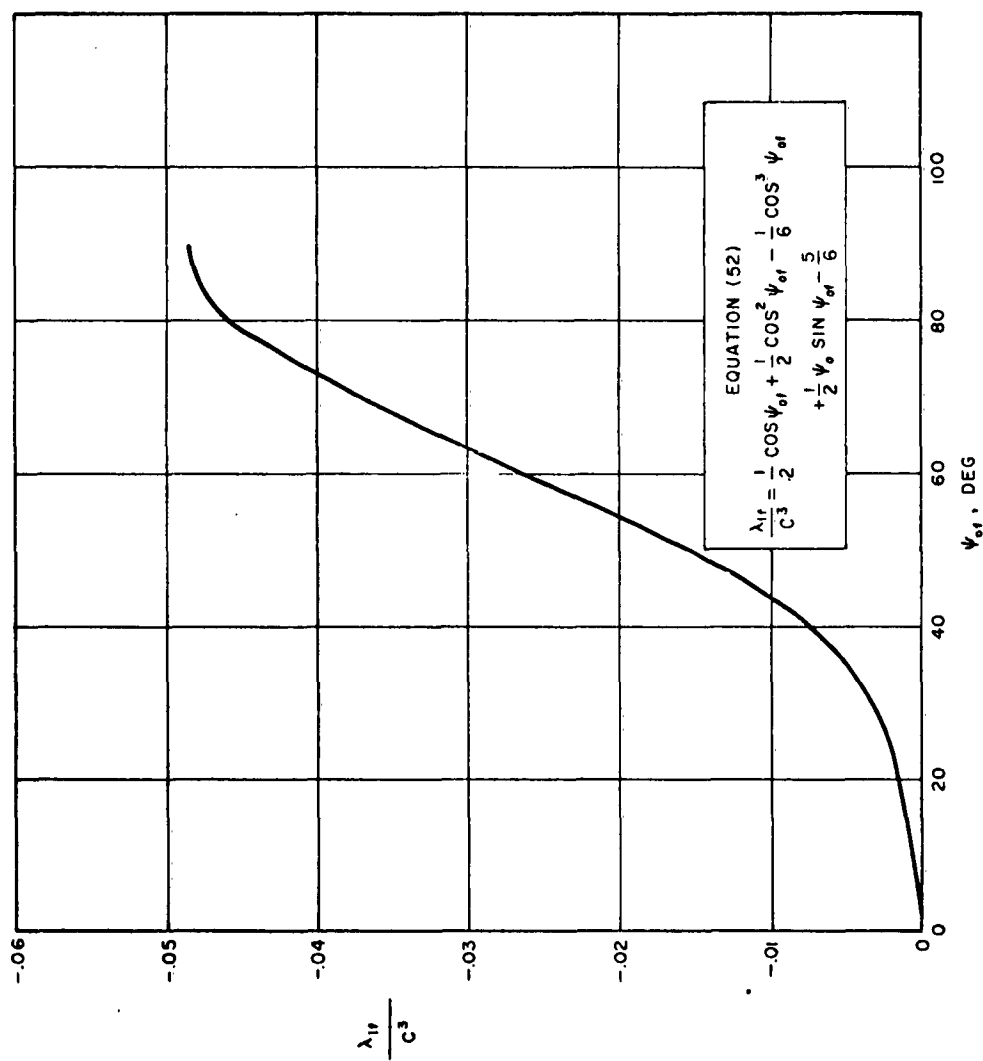
Figure 10. Spherical Earth Correction on Lateral Range Angle.

EQUATION (52)

$$\frac{\lambda_{1f}}{C^3} = \frac{1}{2}\cos\psi_{of} + \frac{1}{2}\cos^2\psi_{of} - \frac{1}{6}\cos^3\psi_{of} + \frac{1}{2}\psi_o \sin\psi_{of} - \frac{5}{6}$$

ψ_{of}, DEG

$\dfrac{\lambda_{1f}}{C^3}$

Table 3. Spherical Earth Correction on Lateral Range Angle
and Lateral Range.

ψ_{Of} (deg)	λ_{1f}/C^3 (radians)	Lateral Range/C^3 (naut mi)
0	0	0
10	- 0.00075	- .2.58
20	- 0.00170	- 5.85
30	- 0.00325	- 11.18
40	- 0.00730	- 25.1
50	- 0.0157.	- 54.0
60	- 0.0266	- 91.5
70	- 0.0365	- 125.5
80	- 0.0458	- 157.5
90	- 0.0483	- 166.0

$$\lambda_f = C \left(1 - \cos \psi_{0f}\right) - C^3 \left(\frac{5}{6} + \frac{1}{6} \cos^3 \psi_{0f} - \frac{1}{2} \cos^2 \psi_{0f} - \frac{1}{2} \cos \psi_{0f} - \frac{1}{2} \psi_{0f} \sin \psi_{0f}\right)$$

(53)

Equation (53) is plotted in Figures 5a, 5b and 5c as the dashed lines and is compared with the exact numerical solutions from Reference 5. The comparison shows that the corrected λ expression can predict the lateral range very closely for most cases. One interesting thing is that whenever the spherical earth correction is negligible in the exact numerical solutions, it is also negligible in the approximate solutions. When the spherical earth correction is large, the approximate solution deviates from the exact numerical solution no more than 10 per cent in the range compared. As for the maximum lateral range, it has been noted in the flat earth solutions that there is no maximum beyond a certain V_i. With the spherical earth correction, the maximum lateral range at low V_i is not affected but a maximum exists at high V_i due to the correction. This fact has been observed in the exact numerical solutions. It can now be concluded that the maxima at low initial velocities are caused by the integrated lateral aerodynamic force while those at high initial velocities are caused by the spherical earth effect. This indicates the importance of the spherical earth correction at high initial velocities.

The spherical earth correction on the down range angle μ is found as follows. Taking Equation (12) and substituting ψ by $\psi_0 + \psi_1$ and λ by $\lambda_0 + \lambda_1$, one gets

$$-\frac{d\mu}{dX} = \frac{2B}{V_s^2} \frac{\cos (\psi_0 + \psi_1)}{\cos (\lambda_0 + \lambda_1)}$$

(54)

or

$$-\frac{d\mu}{dX} = \frac{2B}{V_s^2} \frac{\cos \psi_0}{\cos \lambda_0} \left(\frac{\cos \psi_1 - \tan \psi_0 \sin \psi_1}{\cos \lambda_1 - \tan \lambda_0 \sin \lambda_1}\right)$$

(55)

Since ψ_1 and λ_1 are small, one can write

$$\cos \psi_1 = \cos \lambda_1 = 1, \quad \sin \psi_1 = \psi_1, \quad \sin \lambda_1 = \lambda_1$$

(56)

and Equation (55) becomes

$$-\frac{d\mu}{dX} = \frac{2B}{V_s^2} \frac{\cos \psi_0}{\cos \lambda_0} \left(\frac{1 - \psi_1 \tan \psi_0}{1 - \lambda_1 \tan \lambda_0} \right)$$ (57)

Since λ_1 is always small and λ_0 very rarely reaches beyond 45 degrees, one can assume

$$\lambda_1 \tan \lambda_0 \ll 1$$ (58)

thus

$$-\frac{d\mu}{dX} = \frac{2B}{V_s^2} \frac{\cos \psi_0}{\cos \lambda_0} (1 - \psi_1 \tan \psi_0)$$ (59)

Writing $\mu = \mu_0 + \mu_1$ and substituting in the above, one gets

$$\frac{d\mu_1}{dX} = \frac{2B}{V_s^2} \left(\frac{\psi_1 \sin \psi_0}{\cos \lambda_0} \right)$$ (60

and by Equation (16),

$$d\mu_1 = - C \psi_1 \frac{\sin \psi_0}{\cos \lambda_0} d\psi_0$$ (61)

Using the approximation $\cos \lambda_0 = 1$ which has been proven adequate in computing the down range, one gets

$$d\mu_1 = - C \psi_1 \sin \psi_0 d\psi_0$$ (62)

or

$$d\mu_1 = C^3 \left(\sin \psi_0 - \frac{\psi_0}{2} - \frac{\sin 2 \psi_0}{4} \right) \sin \psi_0 d\psi_0$$ (63)

The initial condition is $\mu_1 = 0$ at $\psi_0 = 0$. Integrating Equation (63), one gets

$$\mu_{1f} = C^3 \left[\frac{1}{2} (1 + \cos \psi_{0f}) (\psi_{0f} - \sin \psi_{0f}) - \frac{1}{6} \sin^3 \psi_{0f} \right] \tag{64}$$

Equation (64) is plotted in Figure 11 and also tabulated in Table 4. It is noted that μ_{1f} is positive and proportional to C^3. Using this correction, the approximate spherical earth solution for down range is

$$\mu_f = C \sin \psi_{0f} + C^3 \left[\frac{1}{2} (1 + \cos \psi_{0f}) (\psi_{0f} - \sin \psi_{0f}) - \frac{1}{6} \sin^3 \psi_{0f} \right] \tag{65}$$

The corrected down range is plotted in Figures 8a, 8b and 8c as the dashed lines. The comparison with exact numerical solutions is quite satisfactory.
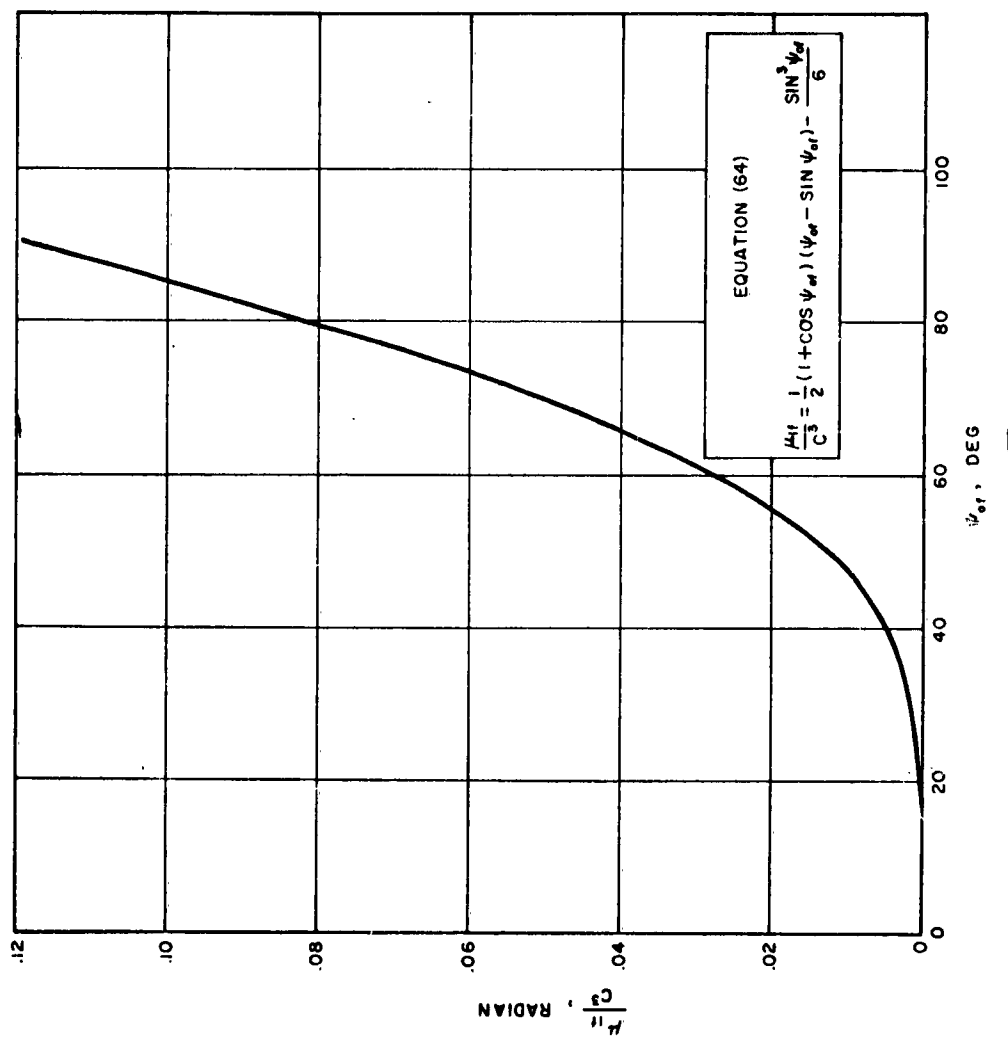
Figure 11. Spherical Earth Correction on Down Range Angle.

Table 4. Spherical Earth Correction on Down Range Angle
and Down Range.

ψ_{0f} (deg)	μ_{1f}/C^3 (radians)	Down Range/C^3 (naut mi)
0	0	0
10	0.00001	0.0344
20	0.00022	0.7560
30	0.00119	4.10
40	0.0045	15.50
50	0.0126	43.40
60	0.0276	95.00
70	0.0507	174.20
80	0.0823	283.00
90	0.1187	407.50

V. CONCLUDING REMARKS

An analytic study has been made of the lateral motion of a re-entry vehicle gliding at a constant altitude. The constant altitude is maintained by banking the vehicle about the velocity vector at a constant angle of attack. The analytic approximate solutions have been compared with numerical exact solutions. It has been shown that the approximate solutions predict higher turn angle, higher lateral range but lower down range. The accuracy of the prediction is generally satisfactory. Among the three variables, the lateral and down range can be predicted well within 10 per cent while the turn angle, with lower accuracy.

There are two important features about these approximate solutions. First, they are simple and can be readily applied to preliminary design work. Secondly, they preserve the characteristics and provide a good understanding of a constant altitude glide.

The results of the approximate solutions show (and the exact numerical solutions agree) that the lateral range, being a function of $W/(C_D A \rho)$ at a given L/D and V_i, exhibits a maximum. The maximum exists for all initial velocities in the case of a spherical earth. For a flat earth it exists at low initial velocities only. The spherical earth correction has been shown to be small for low $W/(C_D A \rho)$, L/D and V_i and become significant only when these parameters assume high values.

APPENDIX A

SUMMARY OF APPROXIMATE SOLUTIONS

I. TOTAL FLIGHT TIME (EXACT)

$$t_f = \frac{L}{D} \frac{C}{g} V_s \left(\sqrt{1 + \frac{1}{C}} - \frac{V_s}{V_i} \right)$$

where

$$C = \frac{2W}{C_L A \rho V_s^2}$$

II. FINAL VELOCITY (EXACT)

$$V_f = \frac{V_s}{-\sqrt{1 + \frac{1}{C}}}$$

III. FLAT EARTH SOLUTIONS

Basic approximation:

$$\sin \phi = 1$$

Final turn angle:

$$\psi_{0f} = \frac{L}{D} \ln \left(\frac{V_i}{V_s} \sqrt{1 + \frac{1}{C}} \right)$$

Final lateral range angle:

$$\lambda_{0f} = C (1 - \cos \psi_{0f})$$

Final down range angle:

$$\mu_{0f} = C \sin \psi_{0f}$$

C* for maximum lateral range:

$$\left(\frac{1}{2}\frac{L}{D}\right)\left(\ln\frac{V_i}{V_s}\sqrt{1+\frac{1}{C^*}}\right) = \text{arc tan}\left(\frac{\frac{1}{2}\frac{L}{D}}{1+C^*}\right)$$

Maximum lateral range

$$\lambda_{0f}^* = \left(\frac{1}{2}\frac{L}{D}\right)\frac{\sin\left[\frac{L}{D}\ln\left(\frac{V_i}{V_s}\sqrt{1+\frac{1}{C^*}}\right)\right]}{1+\frac{1}{C^*}}$$

C* for maximum down range

$$\left(\frac{L}{D}\right)\ln\left(\frac{V_i}{V_s}\sqrt{1+\frac{1}{C^*}}\right) = \text{arc tan}\left(\frac{\frac{1}{2}\frac{L}{D}}{1+C^*}\right)$$

Maximum down range

$$\mu_{0f}^* = \frac{1}{2}\frac{L}{D}\frac{\cos\left[\frac{L}{D}\ln\left(\frac{V_i}{V_s}\sqrt{1+\frac{1}{C^*}}\right)\right]}{1+\frac{1}{C^*}}$$

IV. SPHERICAL EARTH CORRECTION

Correction on final turn angle

$$\psi_{1f} = -C^2\left(\sin\psi_{0f} - \frac{1}{2}\psi_{0f} - \frac{1}{4}\sin 2\psi_{0f}\right)$$

Correction on final lateral range

$$\lambda_{1f} = -C^3\left(\frac{5}{6}+\frac{1}{6}\cos^3\psi_{0f} - \frac{1}{2}\cos^2\psi_{0f} - \frac{1}{2}\cos\psi_{0f} - \frac{1}{2}\psi_{0f}\sin\psi_{0f}\right)$$

Correction on final down range

$$\mu_{1f} = C^3\left[\frac{1}{2}(1+\cos\psi_{0f})(\psi_{0f} - \sin\psi_{0f}) - \frac{1}{6}\sin^3\psi_{0f}\right]$$

APPENDIX B

DISCUSSION OF THE APPROXIMATE SOLUTIONS
FOR VERY SMALL C[+]

It has been mentioned in the text that the $\sin \phi = 1$ approximation becomes more accurate when C gets smaller. The text also shows that the spherical earth correction becomes negligible when C is very small. Furthermore, the lateral range angle λ must be small for small C (λ is proportional to C) and as a result the $\cos \lambda = 1$ approximation used in computing the down range angle becomes more accurate as C gets smaller. Therefore, for very small C, Equations (10), (11) and (12) can be written, with high degree of accuracy, as

$$- \frac{d\psi}{dX} = \frac{L}{D} \tag{B-1}$$

$$- \frac{d\lambda}{dX} = \frac{2B}{V_s^2} \sin \psi \tag{B-2}$$

$$- \frac{d\mu}{dX} = \frac{2B}{V_s^2} \cos \psi \tag{B-3}$$

The solutions of these equations are:

$$\psi = \frac{L}{D} \ln \left(\frac{V_i}{V} \right) \tag{B-4}$$

$$\lambda = C (1 - \cos \psi) \tag{B-5}$$

$$\mu = C \sin \psi \tag{B-6}$$

Combining Equations (B-5) and (B-6), one gets

$$(\lambda - C)^2 + \mu^2 = C^2 \tag{B-7}$$

Equation (B-7) represents a circle with its center at $\lambda = C$ and its radius equal to C . Such a circle is plotted in Figure B-1. The tangent at any point on the circumference of the circle makes an angle ψ with the $\lambda = 0$ line. The line of $\lambda = 0$ is along the original heading of the vehicle and ψ must be the turn angle. Figure B-1 clearly indicates that the vehicle, while making a constant altitude turn, describes a circular path. Depending on the aerodynamics, the mass characteristics and the altitude, the vehicle may find itself anywhere along the circumference of the circle at the end of the turn. The final turn angle has been given by Equation (21) as

$$\psi_f = \frac{L}{D} \ln \left(\frac{V_i}{V_s} \sqrt{1 + \frac{1}{C}} \right) \tag{B-8}$$

Here we drop the subscript 0 because Equation (B-8) can now be applied to a spherical earth also. In the main text, most computations were made for $\psi_f < 90^\circ$. When C is very small, however, the final turn angle can be greater than 90 degrees. If $\psi_f = 180^\circ$, the vehicle would have made a lateral displacement of 2C with no forward displacement and would fly from that instant on in the opposite direction to the original heading. If $\psi_f = 360^\circ$, the vehicle would have made a full 360-degree turn and find itself back to the original location at a much lower velocity. In such case, the vehicle would be dissipating its kinetic energy through drag while turning and it would have no loss in altitude and no gain in either the longitudinal or lateral displacement at the end of the turn.

While maneuvers of 180-degree and 360-degree turn appear to be extremely interesting, the obvious question that has to be answered is whether or not it is practical. To answer this question, we examine a vehicle with $L/D = 2$, $W/C_L A = 25$ lb/ft^2 , at $V_i = 32,000$ ft/sec . In order to have $\psi_f = 180^\circ$,

the turn must be performed at an altitude of 184,000 feet. For a 360-degree turn, the altitude must be 104,000 feet. The corresponding value of C is 0.0704 and 0.00282, respectively. The radius of the turn becomes 242 nautical miles and 9.7 nautical miles, respectively. The centrifugal force created by these turns is in the tens of g's for $\psi_f = 180°$ and in the hundreds of g's for $\psi_f = 360°$. For lower L/D, higher $W/C_L A$ and lower V_i, it becomes more difficult to perform such turns in the sense that the altitude will be lower and the centrifugal force will be higher. Thus, one is led to conclude at this time that constant altitude turns at very small values of C are not likely to be practical.

The above discussion does clarify the statement made in the text about the incorrectness of the curves of lateral range and down range at very small $W/(C_D A \rho)$ as shown in Figures 5 and 8. As one can see from Figure B-1, the lateral range and down range must have the characteristics of a damped oscillation as $W/(C_D A \rho)$ goes to zero. This is schematically shown in Figure B-2. Because of the smallness of the region in which the damped oscillation character occurs, it was not shown in Figures 5 and 8 to avoid confusion.
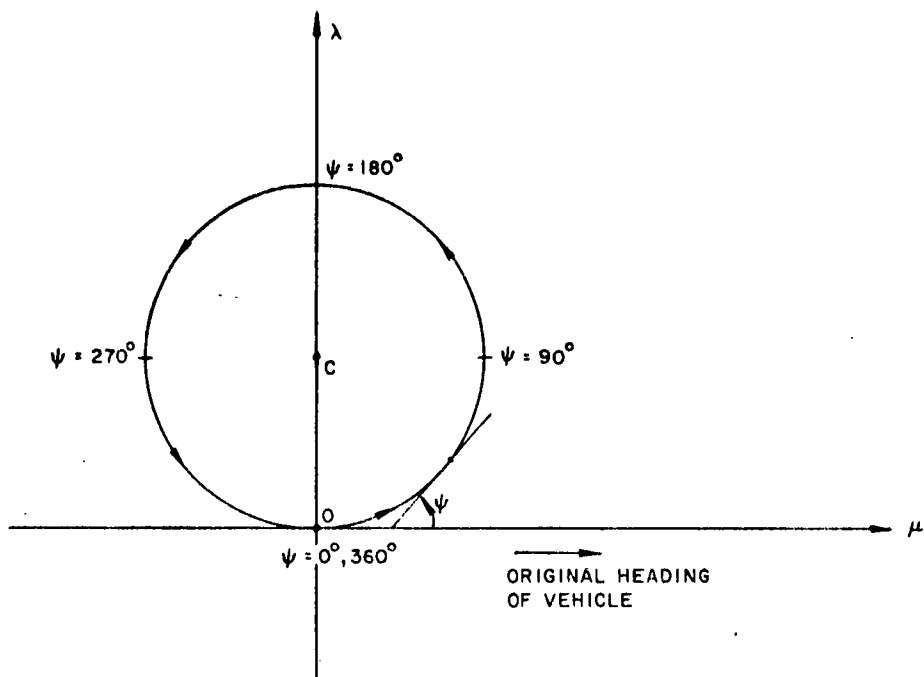
Figure B-1. Vehicle Flight Path at Very Small C .
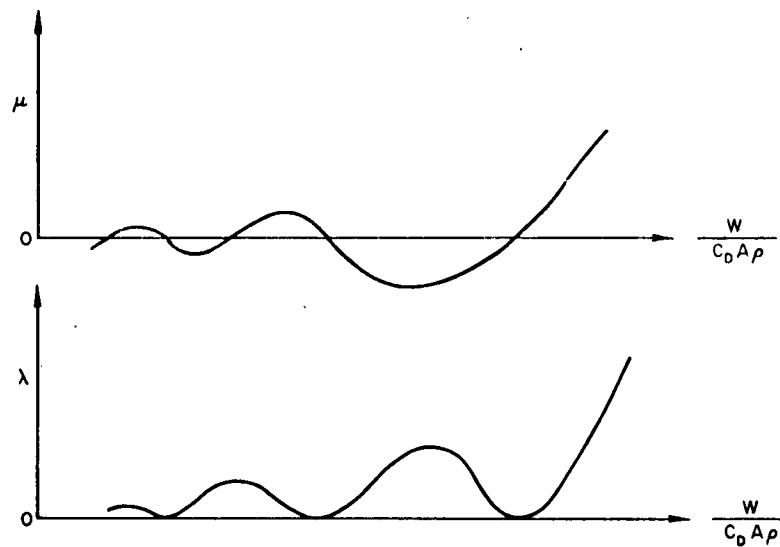
Figure B-2. Schematics of the Variation of λ and μ
with $W/(C_D A \rho)$ at Very Small C .

NOMENCLATURE

A = reference area

B = abbreviation for $W/(C_D A \rho)$

C = abbreviation for $2 B/(L/D) V_s^2$

C_D = drag coefficient

D = drag force

g = gravitational acceleration

L = aerodynamic force perpendicular to drag

t = time

V = velocity

V_s = orbital velocity (= 26,000 ft/sec for earth)

W = vehicle weight

X = abbreviation for $\ln V$

λ = lateral range angle

μ = down range angle

ρ = atmospheric density

ϕ = bank angle

ψ = turn angle

Subscripts

0 = "flat earth" solution

1 = spherical earth correction

f = at the end of the constant altitude glide

i = initial condition

Superscripts

$*$ = maximum

REFERENCES

1. Slye, R. E., "An Analytical Method for Studying the Lateral Motion of Atmosphere Entry Vehicles", NASA TN D-325, September 1960.

2. Smith, R. H. and J. A. Menard, "Superorbital Entry and Recovery with Maneuverable Manned Vehicles", Aerospace Engineering, p 12, October 1961.

3. Ferri, A. and L. Ting, "Practical Aspects of Re-entry Problems", Polytechnic Institute of Brooklyn, PIBAL Report No. 705, July 1961.

4. Wang, H. E. and S. T. Chu, "Variable Lift Re-entry at Superorbital and Orbital Speeds", Presented at IAS Summer Meetings, Los Angeles, Paper No. 62-165, 19-22 June 1962.

5. Skulsky, R. S., "Study of a Particular Lateral Range Re-entry Maneuver", Martin Company, TM 1364-61-16, August 1961.

6. Wang, H. E. and R. S. Skulsky, "Characteristics of Lateral Range During Constant Altitude Glide", to be published in the Journal of Aerospace Sciences.

7. London, H. S., "Change of Satellite Orbit Plane by Aerodynamic Maneuvering", Journal of Aerospace Sciences, Vol 29, No. 3, p 323, March 1962.

8. Love, J. A. and L. W. Neustadt, "Derivation of Three-Dimensional Trajectory Equations for a Lifting Re-entry Vehicle", Space Technology Laboratories, Interoffice Correspondence 7431.1-107, 9 November 1960.

9. Wang, H. E., "On the Three-Dimensional Equations of Motion of a Lifting Re-entry Vehicle Over a Non-Rotating Spherical Earth", Aerospace Corporation Interoffice Correspondence A62-1761-225, 8 November 1962.

10. Skulsky, R. S., Aerospace Corporation Report to be published.

11. Jackson, W. S., "An Improved Method for Determining the Lateral Range of a Gliding Entry Vehicle", Reader's Forum, Journal of Aerospace Sciences, Vol 28, No. 11, p 910, November 1961.

12. London, H. S., "Comments on Lateral Range During Equilibrium Glide", Reader's Forum, Journal of Aerospace Sciences, Vol 29, No. 5, p 610, May 1962.

Aerospace Corporation, El Segundo, California.
APPROXIMATE SOLUTIONS OF THE LATERAL
MOTION OF RE-ENTRY VEHICLES DURING
CONSTANT ALTITUDE GLIDE by H. E. Wang.
25 February 1963. 55 pages including illustrations.
(Report TDR-169(3560-10)TN-1, SSD-TDR-63-60)
Contract No. AF04(695)-169.

Unclassified Report

Approximate analytic solutions have been obtained
to the lateral motion of re-entry vehicles during
constant altitude glide. The constant altitude glide
is maintained by banking the vehicle about its ve-
locity vector at a fixed angle of attack. Such a
glide mode is often used in design studies to
achieve lateral range but no simple analytic solu-
tions have been available up to now. The approach
taken here is to first treat the "flat earth" case
and then include the spherical earth correction.

(over)

Aerospace Corporation, El Segundo, California.
APPROXIMATE SOLUTIONS OF THE LATERAL
MOTION OF RE-ENTRY VEHICLES DURING
CONSTANT ALTITUDE GLIDE by H. E. Wang.
25 February 1963. 55 pages including illustrations.
(Report TDR-169(3560-10)TN-1, SSD-TDR-63-60)
Contract No. AF04(695)-169.

Unclassified Report

Approximate analytic solutions have been obtained
to the lateral motion of re-entry vehicles during
constant altitude glide. The constant altitude glide
is maintained by banking the vehicle about its ve-
locity vector at a fixed angle of attack. Such a
glide mode is often used in design studies to
achieve lateral range but no simple analytic solu-
tions have been available up to now. The approach
taken here is to first treat the "flat earth" case
and then include the spherical earth correction.

(over)

Simple expressions have been obtained for the turn angle, lateral range angle and the down range angle. A comparison with exact numerical solutions shows that the approximate solutions are sufficiently accurate for preliminary design purposes.

The approximate solutions, although simple, contain all the characteristics of the glide mode in question. The results show that the lateral range, being a function of $W/(C_D A \rho)$, exhibits a maximum for a given L/D and initial velocity for the spherical earth case. In the flat earth case, the maximum exists for suborbital and orbital initial velocities and ceases to exist above a certain initial velocity depending on L/D. The down range also exhibits a maximum for a given L/D and initial velocity provided that the initial velocity is suborbital. The spherical earth correction on the lateral and down range has been shown to be small for low $W/(C_D A \rho)$, L/D and initial velocities and becomes significant when these parameters are high. All these findings agree with exact numerical solutions.